بسم الله الرحمن الرحيم

Sudan University of Science and Technology

College of Post Graduate Studies

Effect of Doping Zinc Oxide and Titanium Oxide Cells with (Al, Cd, Co,Li and Mg) on Optical Properties and Efficiency

تأثيرتشويب خلايا أكسيد الخارصين وأكسيد التتانيوم بعناصر(الألمنيوم و الكادميوم والكوبالت و الليثيوم والماغنزيوم) علي الخواص الضوئية والكفاءة

A Thesis submitted in Fulfillment of the Requirement for the degree of Doctor of Philosophy in Physics

Submitted by:

ShadiaTagEldin Ibrahim ShaaEldin

Supervision: Prof. Dr: Mubarak DirarAbd-Alla

Co- supervision Dr :Sawsan Ahmed Elhouri Ahmed

2019

Dedication

ToMy husband,

My father and Mother,

My dear sisters and brothers,

Acknowledgement

First off all, I would like to thank Allah almighty for making this work possible. Secondly, I would like to express my gratitude to my supervisors Prof.Mubarak DirarAbdallah, Dr.Sawsan Ahmed ElhouriAhmeda, and Dr. AbdalsakhiAbdallah for his supervision, valuable advice, kind treatment and guidance during this work period and chemistry department, colleagues and all whom support me.

Abstract

In this work the optical properties of two group of samples were studied. In the first group Zinc Oxide was doped by (Al ,Cd, Co, Li and Mg). In the second group Titanium Oxide was doped by (Al ,Cd, Co, Li and Mg) also . The optical characteristics where investigated by using UV spectrophotometer and some computer programmers . The efficiency of the solar formed from this samples using ITO were found using light current and voltage .The study shows that the absorption peaks of the samples corresponds to the energy gaps . The solar cells efficiency increases as the energy gap decreases . For TiO_2 doped with CdO_4 ,CoO_2 ,LiO_2 , MgO_2 and Al_2O_3 the beak absorptions are(308 , 308,310, 300 and 510) nm respectively the corresponding energy gaps are (3.688 ,3.42 ,3.482,3.364 and 2.155) eV respectively which shows inverse relation with energy peaks .This agrees with theoretical relations . The Mefficiencies are (0.188, 0.247 ,0.452 ,0.478 and 0.569) % which are inversely related to the energy gap expect for Lithium due to the existence of other factors affecting the efficiency . For Zn O doped with CdO_4 ,CoO_2 ,LiO_2 , MgO_2 and Al_2O_3 the beak absorptions are(290 , 300,302, 305 and 504) nm respectively and the corresponding energy gaps are (3.644 ,3.685 ,3.505,3.687 and 3.699) eV while the corresponding efficiencies are (0.205, 0.204 ,0.297 ,0.191 and 0.168) % . The same comments and relations holds for Titanium holds also for zinc oxide group including Lithium again. It is clear that the efficiencies of TiO_2 samples are higher than that of ZnO . It was also found that the absorption coefficient and theeffeciency increases as the energy gap decreases . These results agrees with many previous studies and theoretical relations.

المستخلص

في هذا البحث درست الخصائص الضوئية لمجموعتين من العينات الأولي هي أكسيد الخارصين الذي طعم بالألمنيوم والكادميوم والكوبالت والليثيوم والماغنزيوم أما المجموعة الثانية أكسيد التيتانيوم فطعمت بنفس العناصر السابقة .تمت دراسة الخصائص الضوئية بواسطة جهاز مطيافية الأشعة فوق البنفسجية وبعض برامج الحاسوب .كفاءة الخلايا المصنعة من هذه المواد حسبت بعد أن تم إستخدام زجاج (**ITO**) وحساب التيار والجهد الضوئيين .أوضحت الدراسة تطابق قيم قمم الامتصاص مع فجوة الطاقة. حيث تزيد كفاءة الخلية بنقصان فجوة الطاقة. بالنسبة لأكسيد التيتانيوم المشوب بمواد (الألمنيوم والكادميوم والكوبالت والليثيوم والماغنزيوم) تكون قمم الإمتصاص هي (308 ,308 , 310 ,305 و 510) نانوميتر بالترتيب . وتكون قيم فجوات الطاقة المناظرة هي (3.688 , 3.42 ,3.482 , 3.364 و 2.155) إلكترون فولت بالترتيب وهي توضح علاقتها العكسية مع قمم الإمتصاص وهذه تتفق مع العلاقات النظرية وتكون قيم الكفاءة المناظرة (0.188 , 0.247 , 0.452 , 0.478 و 0.569) % وهي تتناسب عكسيا مع قيمة فجوة الطاقة بإستثناء الليثيوم لوجود عوامل أخري تؤثر علي الكفاءة . وبالنسبة لأكسيد الخارصين المشوب بمواد (الألمنيوم والكادميوم والكوبالت والليثيوم والماغنزيوم) تكون قمم الإمتصاص هي (290 , 300 , 302 , 305 و 504) نانوميتر وتكون قيم فجوة الطاقة المناظرة (3.644 , 3.685 , 3.505 , 3.687 و3.699) 'إلكترون فولت , في حين تكون قيم الكفاءة المناظرة هي (0.205 , 0.204 , 0.297 , 0.191 و 0.168) % وتنطبق نفس ملاحظات وعلاقات أكسيد التيتانيوم علي أكسيد الخارصين بما فيها شذوذ نتائج الليثيوم . ومن الواضح أن كفاءات عينات أكسيد التيتانيوم أعلي

من أكسيد الخارصين . وكذلك يلاحظ أن معامل الامتصاص يزيد بنقصان فجوة الطاقة والكفاءة تزيد بنقصان فجوة الطاقة ايضا .هذهالعلاقاتتتفقمعالعديدمنالدراساتالسابقةوالعلاقاتالنظرية.

Table of Contents

List of tables

List of Figures

Chapter One

Introduction

1.1Introduction:

Energy is need by people for wide variety of applications .The need of energy in Sudan is rapidly growing. Sudan is the largest in the African continent, with a tropical climate and area of approximately10^6square miles(2.5×10^6 km2). It lies between latitudes 3 and 23ºN; and longitudes 21º 45 E and 39º E this large area enjoys a variety of climates, from desert regions in the north , to tropical in the south , and makes it a favorable environment for all activities of integrated agricultural investment from production to processing industries (Omer , 1995 a) Sudan is a relatively sparsely populated country . The total population according to the census 2008 was 39 $\times 10^6$inhabitants. The annual growth rate is 2.8% , and population density is 14 persons per square kilometer (Omer , 2008) . Sudan is rich in land and water resources (Omer, 1998 a). Sudan has a predominately continental climate, which roughly divides, into three climatologically regions.

Sudan possesses great potentialities for industrialization since it is rich in agricultural raw materials resources. Energy is an essential factor in the development movement, since it stimulates and supports the economic growth, and development. The increasein oil pricesand the pollution it causes ,limits its used widely. The fossil fuels especially oil and natural gas, are finite in extent , and should be regarded as depleting assets.Due to the importance of energy, mostof economic resources are directed to establish sources of energy, many of which now face serious environmental and other constraints. This en courage's some people used as the biomass sources which are increasingly being regarded as a central part of long solutions to the energy environment problem . However

increasing energy services increase exploitingbiomass energy sources and otherenergy resources . In recent years attention had been paid to used renewable solar energy .This be causes it's sustainable and is pollution free .In rural are people uses conventional cheap energy resources . The poor situations of conventional energy supplies to Sudanese people are characterized by high dependence on biomass woody fuels (firewood, and charcoal). More that 70% of the total Sudanese population live in rural and isolated communities characterized by extreme poverty,power social and uneconomical activities (Omer, 1996a). The unavailability and the acute shortages of the conventional energy supply (petroleum and electricity) to rural people forced them to use alternatives available energy sources like biomass (Omer, 1996 b).

The suitable energy source, needed for the rural requirements must be of low cost environmentally, socially and economically acceptable. The urgent problem for rural people development is to increase the energy using solar renewable energy sources .One of the most suitable one is the solar cell which converts radiation to to electric energy. The conventional solar cell is that made of silicon .The wide spread of this cell is limited by its high cost and low efficiency . New research investigates theoretically solar cells based on semiconductor materials such as Ge , Si , Ga As , Inp, Cdte and CDs are considered here .A single junction solar cell has maximum efficiency at an energy gap of around 1.35-1.5 ev .shokly and Quesser showed that the maximum theoretical efficiency of a single solar cell is limited to 33% . However, this limit could be overcome through the used of multiple cells , with varying band gaps , in serial (Tandem) arraignment . Crystalline silicon (si) has been the dominant material for photovoltaic (PV) cells for the past two decades .other low cost semiconductor materials are better suited to absorb he solar energy spectrum and are in development . Some are semiconductor

thin – films such as amorphous silicon (a – si) , copper induium gallium diselenide 9 cu (In Ga) se2 or CIGS) , and direct bandgapsemiconductros from II – VI materials ; e.g., cadmium telluride (Cd Te)and cadmium sulfide(CdS) are good candidates for use in solar cells . Recently the emergence of the so called nano science opens a new horizon in developing solar cells [1]. according to nano science the property of any bulk matter can be changed by disintegrating the bulk matter into very small tiny pecies, isolated, and having dimensions in the range of (1-300) nm ,where 1nm= 1nanometer=10^{-9} m . Such isolated very tiny parts are called nano martial. Since these isolate particles are on the atomic scale .they are on the described by quantum laws so thus one can changed the physical property of nano material by changed it nano structure [2].Thus properties like absorption ,energy gap can be controlled easily for nano martials . Thus one can improve the efficiency of the solar cell by using nano martials in fabricating them .Such cells are cold nano solar cells . Some of these celled used polymer or dyes while other utilization Zinc oxide and copper oxide .The latter types as pacers to be more promising since they are more stable and have long life time comparedto plastic and dye [3].

1.2 Research problems:

The fact that Zinc and Copper oxide cells have long life time and more stability needs doing a lot of work to increase the very low efficiency and performance of them.

1.3Aim of Work :

The aim of this study is to see how to improve ZnO solar cells doped with selected materials from the periodic table of elements groups (II, VI) and (III & V). The study aims also to open a new horizon in fabrication low cost ease fabricated solar cells.

1.4 Thesis Layout:

The thesis consists of the five chapters. Chapter one is the Introduction and Chapter two is the theoretical background aboutcharge transport. Chapter three is the literature Review. Chapter four consists of method, materials, results and analysis. Chapter five is concerned with Conclusion and Recommendations.

Chapter Two

Theoretical Background

2.1 Introduction

Nano solar cells consist of many type .For example photo electrochemical solar cells (PSCs), consisting of a photo electrode, a redox electrolyte, and a counter electrode, have been studied extensively. Many semiconductor materials, including single-crystal and polycrystalline forms have been used as photo electrodes. These materials can produce current conversion efficiency of approximately 10%. However photo corrosion of the electrode in the electrolyte solution frequently occurs, resulting in poor stability of the cell, so efforts have been made to develop more stable PSCs [10].Oxide semiconductor materials have good stability under irradiation in solution. However, stable oxide semiconductors cannot absorb visible light because they have relatively wide band gaps [11].Sensitization of wide band gap oxide semiconductor materials, such as TiO_2, ZnO, and SnO_2, with photosensitizers, such as organic dyes, that can absorb visible light has been extensively studied in relation to the development of photography technology since the late nineteenth century. In the sensitization process, photosensitizers adsorbed onto the semiconductor surface absorb visible light and excited electrons are injected into the conduction band of the semiconductor electrodes. Dye-sensitized oxide semiconductor photo electrodes have been used for PSCs [12]. This chapter is concurred with exhibiting the properties of these now solar cell types .

2.2. Structure of Dye sensitized solar cell

The essential parts of dye sensitized solar cells (DSSCs) systems is composed of five elements, the transparent conducting oxides, counter

conducting electrodes, the nano-structured wide band gab semiconducting layer, the dye molecules (sensitizer), and the electrolyte [13].

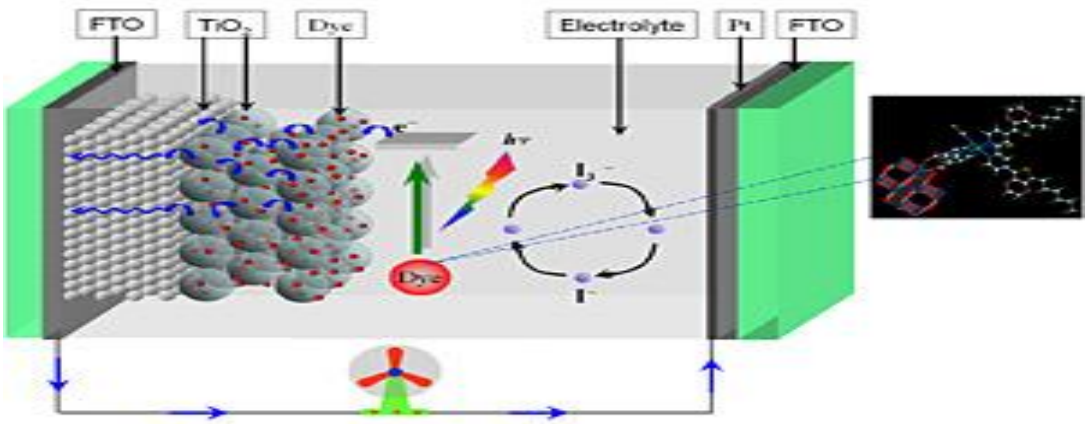

Figure (2.1) Dye sensitized solar cell diagram (source: Dyes sensitized solar cell images).

2.2.1. Transparent conducting oxides (TCO) for both the conducting electrode and counter electrode

TCO coated glass is used as substrate for the TiO2 photo electrode. For high solar cell performance, the substrate must have low sheet resistance and high transparency. In addition, sheet resistance should be nearly independent of the temperature up to 500oC, because sintering of the TiO2 electrode is carried out at 450oC. Fluorine-doped tin oxide (FTO) coated glass is electrically conductive and ideal for use in a wide range of devices, including applications of thin film photo–voltaic devices, it has been recognized as a very promising material because it is relatively stable under atmospheric conditions, chemically inert, mechanically hard, Easily fabricated, has a high tolerance to physical abrasion and is less expensive than indium tin oxide [14].

2.2.2. TiO2photo–electrode

Photo–electrodes made of such materials as Si, GaAs, InP, and CdS decompose under irradiation in solution owing to photo–corrosion. In

contrast, oxide semiconductor materials, especially TiO2, have good chemical stability under visible irradiation in solution; additionally, they are nontoxic and inexpensive. The TiO2 thin-film photo–electrode is prepared by a very simple process. TiO2 colloidal solution (or paste) is coated on a TCO substrate and then sintered at 450 to 500◦C, producing a TiO2 film [15].

2.2.3. The dye molecules (sensitizer)

Dye molecules of proper molecules structure are used to sensitized wide band gab nanostructure photo electrode [16].

2.2.3.1. Types of dyes (Inorganic dye)

Includes metal complex, such as poly pridy (complex of ruthenium and osmium) [17].

- ***Organic dye***

At the last years the efficiency of dye sensitized solar cell with organic dyes has increased comparable to the Ru-complex. Since organic dyes are not based on rare noble metal, the production costs mainly depend on the number of synthesis steps, thus they are potentially very cheap.The absorption coefficients are typically one order of magnitude higher comparable to Ru-complex making very thin TiO2 –layers feasible. At this point none of the organic dyes have proven stability under evaluated temperature .the following examples is the most promising dye classes at the moment [18].

- ***Natural dyes***

Dyes derived from natural materials are exclusively used for educational purpose representing a low–cost and environmentally friendly alternative to conventional Ru-complex. Extracted dyes might also be a good starting point to evaluate, which dyes classes are potentially interesting for sensitization, example of natural dyes blackberries gave a conversion efficiency of 0.056% [11]

- ***Organic complex of other metals:***

Other metal complex have been securitized for their application in DSSC, among them Os- ,Pt ,and Fe-complex .however the overall conversion efficiency is only 50% of standard Ru-dye .Pt-complex give modes efficiencies of 0.7% and iron-complex ,which are very interesting due to the vast abundance of the metal and its non-toxicity are at a very low efficiency level at the moment 0.3% [19].

2.2.4. Electrolytes

Electrolyte containing I-/I-3 redox ions is used in DSSC to generate the oxidized dye molecules and hence completing the electric circuit by mediating electrons between the nanostructure electrode and counter electrode [20].

2.3. Dye–sensitized Solar cell parameters

The percentage power conversion efficiency (PCE) or of any solar cell device is simply the ratio of power output (Pout) versus power input ,(Pin) , power input (Pin) depend upon the incident light flux(Io), and Power output implicit properties of the device itself ;namely the short-circuit current (Isc) open-sir cut voltage (Voc) and fill-factor (FF).the short-circuit current density (Jsc)is typically reported to allow comparison between devices whose dimensions may vary (Jsc=Isc/area) .the FFis determined by the ratio maximum obtainable power/theoretical obtainable power where the theoretical obtainable power is the product Isc,Voc (Isc and Voc being zero at open –circuit and short- circuit condition respectively with grade A solar –cells typically having (FF =0.7) [21].

$$FF = \frac{Imax\ Vmax}{IscVoc} \quad \% \qquad (2.1)$$

$$PCE = \eta = \frac{Pout}{Pin} \times 100 = \frac{IscVoc\,FF}{I000\,A} \times 100 \qquad (2.2)$$

2.4 Comparison of Common Types of PV modules

Silicon is a material commonly used in commercial PV modules. It is the second most abundant element in the Earth's crust, oxygen is the most abundant. Silicon occurs most frequently in nature as silicon dioxide (silica, SiO2) and as silicates (compounds containing silicon, oxygen, metals, and maybe hydrogen). Sand and quartz are two of its most common forms. However, sand is generally too impure to be processed into silicon. High-grade deposits of quartzite can be almost 99% pure silica, but will still be less than 90% silicon. The silica must be processed to become silicon. To become semiconductor grade silicon it must be processed and purified until it is 99.9999% pure silicon! This process, as you might expect, is very expensive. The computer industry uses purified silicon for manufacturing its computer chips [22].

2.4.1 Single crystal silicon (the Siemens modules on your roof are single crystal silicon)

Advantages

• Well established and tested technology

• Stable conversion efficiencies over the life (20-30 years) of the module

• Highest efficiencies of silicon solar cells

Disadvantages

• Expensive manufacturing process

• Uses expensive single crystal and other materials

• Round crystals have less packing density (single crystal silicon ingots are pulled from molten silicon as cylinders that are sawed into wafers

Fig (2.2) Single crystal silicon (the Siemens modules on your roof are single crystal silicon)

2.4.2 Polycrystalline Silicon

Advantages

• Well established and tested technology

• Stable conversion efficiencies over the life (20-30 years) of the module

• Square cells for better packing density

Disadvantages

• Uses expensive materials (though less expensive than single crystal silicon)

• Expensive manufacturing process

• Slightly less efficient than single crystal silicon

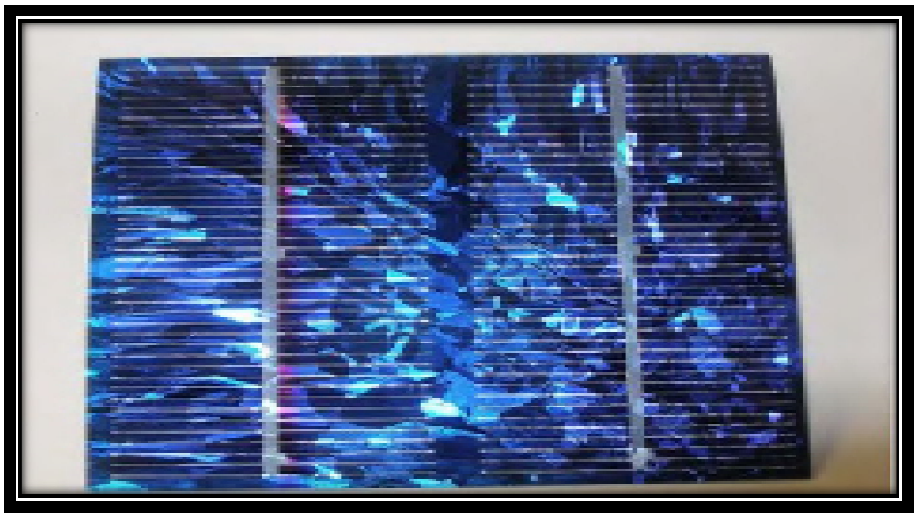

Fig (2.3) Polycrystalline Silicon solar cell

2.4.3 Amorphous Silicon

Advantages

• Low material use because the films are microns thick

• Potential for automated production

• Potential for low cost

• Less affected by shading due to long, thin cells – harder to shade a single cell

• Thinness contributes to use in specialized applications, i.e. calculators and watches (where small amount of power is required)

• Can be incorporated into windows and roofing tiles or shingles in building-integrated PV systems (the electrical generation system is part of the building skin)

Disadvantages

• Lower efficiencies than single and polycrystalline silicon

• Larger areas needed for same power output as single or polycrystalline silicon due to lower efficiencies the cost per unit area (cost/area) of silicon solar cells increases with the size of the crystals. This means that a smaller area of single-crystal cells is required to generate 100 W of

power. The cost of a panel that will generate a 100 W may be more constant than the size[23].

Fig (2.4) Amorphous Silicon solar cells

2.4.4 Other Materials for PV Cells

Other materials are being researched for both their electrical generation potential and commercial feasibility, including: Copper Indium Dieseline, Cadmium Telluride, and Gallium Arsenide. These compounds may become the PV material of choice in the future [24].

2.5 Dyes solar cell

The dye-sensitized solar cells (DSSC) provide a technically and economically credible alternative concept to present day p–n junction photovoltaic devices. These devices are based on the concept of charge separation at an interface of two materials of different conduction mechanism. To date this field has been dominated by solid-state junction devices, usually made of silicon, and profiting from the experience and material availability resulting from the semiconductor industry. The dominance of the photovoltaic field by inorganic solid-state junction devices is now being challenged by the emergence of a third generation of cells [27].

2.5.1Structure of Dye sensitized solar cell

The main parts of DSSCs systems is composed of five elements, the transparent conducting oxides, counter conducting electrodes, the nano-structured wide band gab semiconducting layer, the dye molecules (sensitizer), and the electrolyte Transparent conducting oxides (TCO) for both the conducting electrode and counter electrode TCO coated glass is used as substrate for the TiO2 photo electrode. For high solar cell performance, the substrate must have low sheet resistance and high transparency. In addition, sheet resistance should be nearly independent of the temperature up to 500oC, because sintering of the TiO2 electrode is carried out at 450oC. Fluorine-doped tin oxide (FTO) coated glass is electrically conductive and ideal for use in a wide range of devices, including applications of thin film photo–voltaic devices, it has been recognized as a very promising material because it is relatively stable under atmospheric conditions, chemically inert, mechanically hard, Easily fabricated, has a high tolerance to physical abrasion and is less expensive than indium tin oxide [28].TiO2photo–electrode Photo–electrodes made of such materials as Si, Ga As, In P, and Cd S decompose under irradiation in solution owing to photo–corrosion. In contrast, oxide semiconductor materials, especially TiO2, have good chemical stability under visible irradiation in solution; additionally, they are nontoxic and inexpensive. The TiO2 thin-film photo–electrode is prepared by a very simple process. TiO2 colloidal solution (or paste) is coated on a TCO substrate and then sintered at 450 to 500◦C, producing a TiO2 film [29]. The dye molecules (sensitizer) Dye molecules of proper molecules structure are used to sensitized wide band gab nanostructure photo electrode [30].

2.5.2 Types of Organic Solar Cells:

They are some types such as:

Dye sensitized solar cells: Electrochemical cells.

Polymer solar cells: Made by solution, low temperature processing.

2.5.2.1 Dye Sensitized Solar Cells:

In 1991 Brian O'Regan and Michael Grätzel introduced the dye sensitized solar cell (DSSC). This type of solar cell is considered as accost effective alternative for silicon solar cells. The heart of the DSSC is a high surface area TiO2 nano particulate electrode, covered with a monolayer of dye molecules. Upon photo excitation of the dye an electron is injected into the conduction band of the TiO2. A redox couple (I-/I3-) in an electrolyte.

Solution covering the whole TiO2 electrode regenerates the dye, and is itself in return regenerated at the counter electrode. The layout of the DSSC is shown in figure (2.6). Often, transition metal complexes are used as dyes, e.g. RuL2-(NCS)2 (known asN3 dyes), where L is a π-conjugated ligand with TiO2 anchoring groups. The best DSSCs reach efficiencies higher than 10% measured under AM1.5 solar irradiation. The main drawback of the traditional DSSC, hampering wide use, is the application of a liquid electrolyte. This liquid electrolyte is often related to its poor thermo-stability, and responsible for the corrosion of the Pt covered counter electrode. For this reason alternatives for an electrolyte are being developed, aiming at solid-state version of the DSSC. Current state of the art quasi-solid-state dye, Figure 2.6Schematic scheme of the traditional dye sensitized solar cell. Sensitized solar cells based on the iodide/triiodide redox couple, reach stable and > 6% efficient solar cells. Commercial application of this type of solar cells in consumer products is currently explored by Hitachi Maxell for application in a film-like lightweight solar battery. One recent result, also by the Grätzel group, is a solvent-free dye-sensitized solar cell based on an ionic liquid electrolyte and using Se CN-/ (Se CN)3- as the redox couple, replacing the

iodide/triiodide redox couple. This solar cell reaches measured AM1.5 efficiencies of 8%. Another elegant example of recent progress is the quasi solid-state tandem DSSC developed by Dürr and coworkers. The device layout and working Principles are shown in figure 2.8. Two separate dye-sensitized cells are connected in parallel and placed on top of each other. The cell first exposed to illumination contains a Red dye, the other a so called black dye. This assures an effective absorption of the solar emission, leading to a high power conversion efficiency of 10.5%, measured under AM1.5 conditions [30].

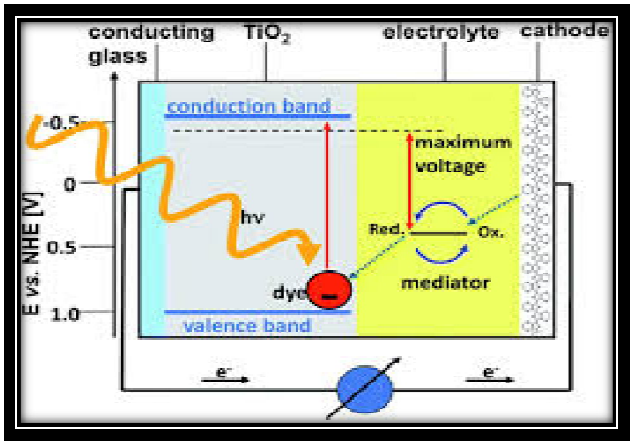

Fig (2.5) Schematic scheme of the traditional dye-Sensitized solar cell

2.5.2.2 Polymer Solar Cells:

A polymer solar cell is a type of flexible solar cell made with polymers, large molecules with repeating structural units, that produce electricity from sunlight by the photovoltaic effect. Polymer solar cells include organic solar cells (also called "plastic solar cells"). They are one type of thin film solar cell, others include the currently more stable amorphous silicon solar cell [31]. Polymer solar cell technology is relatively new and is currently being very actively researched by universities, national laboratories, and companies around the world. Compared to silicon-based devices, polymer solar cells are lightweight (which is important for small

autonomous sensors), potentially disposable and inexpensive to fabricate (sometimes using printed electronics), flexible, and customizable on the molecular level, and they have lower potential for negative environmental impact. An example device is shown in Fig. 1. The disadvantages of polymer solar cells are also serious: they offer about 1/3 of the efficiency of hard materials, and they are relatively unstable toward photochemical degradation. For these reasons, despite continuing advances in semiconducting polymers, the vast majority of solar cells rely on inorganic materials. Polymer solar cells currently suffer from a lack of enough efficiency for large scale applications and stability problems but their promise of extremely cheap production and eventually high efficiency values has led them to be one of the most popular fields in solar cell research. It is worth mentioning that state-of-the-art devices produced in academic labs – with the record currently held by Yang Yang's group in UCLA – have reached certified efficiencies above 8% while devices produced which have remained unpublished – probably to maintain secrecy for industrial applications – are known to have already gone above 10% [32].

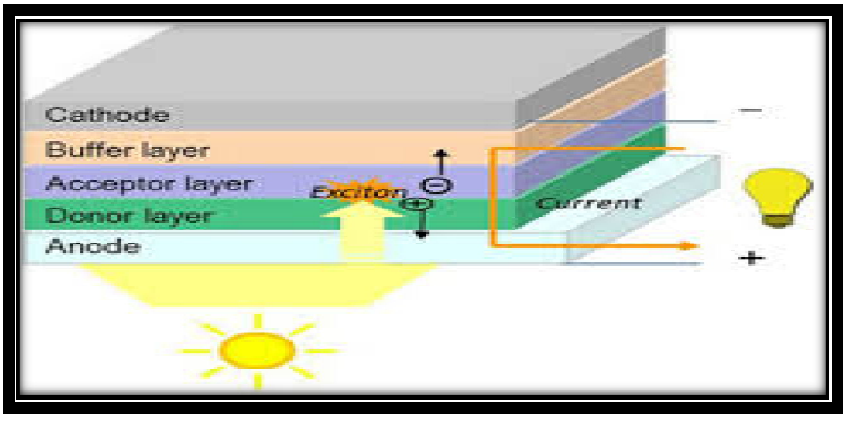

Fig (2.6) Polymer solar cells

2.5.2.3 Polymer Solar Cells Work:

Like all solar cells, the polymer solar cell converts light into electricity, by converting a flux of photons (light) into a flux of charged particles (a

current). This conversion process is made possible by the combination of several types of materials, all having distinct electrical and optical characteristics as described in the text presenting the polymer solar cell layer stack, but most importantly is the inclusion of semiconductors. explain how polymer solar cell is able to generate electricity, and will do so in three sections signifying the three main steps of the conversion process which can be summarized in brief.

A photon incident on a semiconductor, having an energy that exceeds the semiconductor band gap, excites an electron to an unoccupied state above band gap, creating an electron-hole (e-h) pair. The electron-hole pair is subsequently separated over a built-in gradient in the electrochemical potential of the solar cell. Finally, the electron and hole is collected at opposite electrodes and led to recombine after being put to work in an external circuit [33].

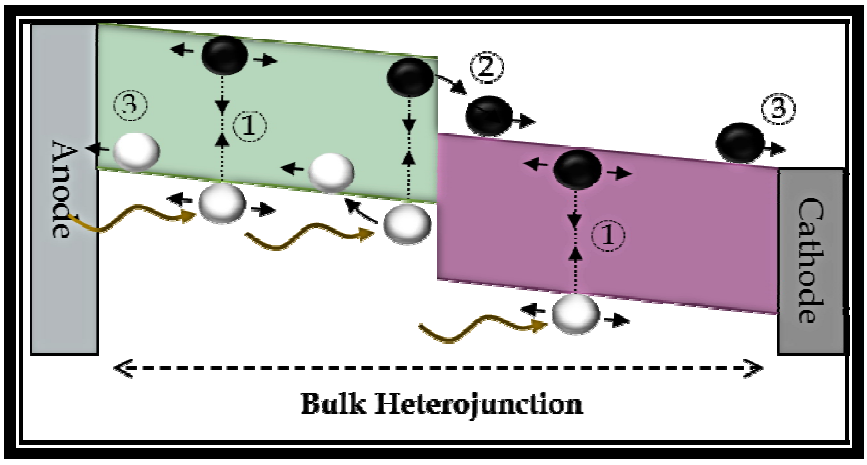

Figure (2.7). The working principle

The working principle of the solar cell. Light enters the cell through the transparent anode, and is absorbed in the bulk heterojunction layer through generation of excitons (1). The excitons diffuse in the bulk heterojunction until they either recombine or reach a donor-acceptor interface, where they separate into electrons (black) and holes (white) (2).

The electrons and holes will then move to the respective anode and cathode, through the donor and acceptor material phase (3) [33].

2.5.2.4 Consist of Polymer Solar Cell:

Making a polymer solar cell is often done using polymers dissolved in organic solvents, which are transferred by printing or coating methods to a substrate. The materials are added in layers in a certain order to build a solar cell stack. The materials needed in the solar cell stack are; a central active (light absorbing) layer, which translate the impinging photons into separate electrons and holes, a selective charge transport layer on each side of the active layer, allowing only passage of either electrons (ETL) or holes (HTL), and finally two electrodes for extracting the charges from the solar cell, with at least one of the electrodes having a requirement of transparency such that the light can pass through and reach the active layer [34].

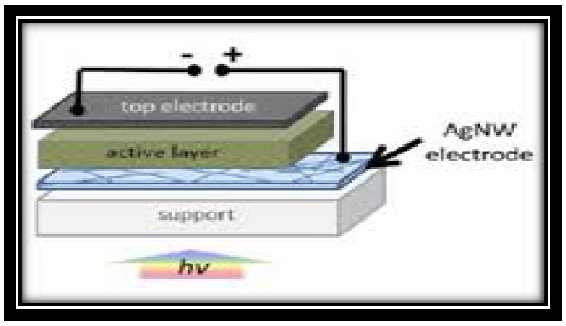

Fig (2.8) Consist of Polymer Solar Cell

2.6 Geometries:

Polymer solar cells are often divided into two groups based on the solar cell stack geometry. A normal and an inverted geometry. The definition of the two geometries lies within the direction of the charge flow. In a normal geometry solar cell the substrate and the transparent electrode on it is the positive electrode, with the light passing through the substrate and this electrode before being absorbed in the active layer. The top electrode is then the negative electrode. In the inverted geometry the two

electrodes and the charge selective layers are switched around, such that the transparent electrode at the substrate is the negative electrode, with a ETL layer between it and the active layer, while the top electrode is the positive electrode with a HTL layer between it and the active layer [35].

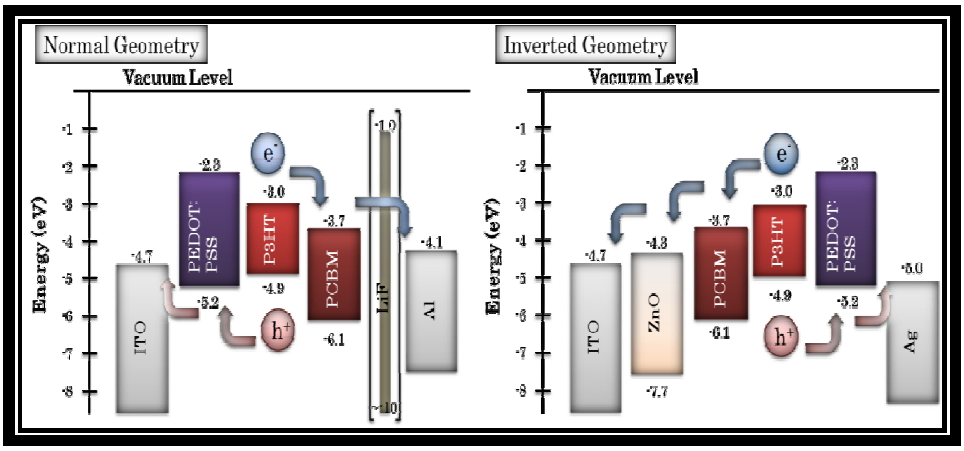

Fig (2.9) Energy levels for normal and inverted geometry solar cells

2.7 Active layer:

The active layer consists of two components in the polymer solar cells. A donor which absorbs the light and an acceptor which extracts the electron from the excitonic bound electron hole, resulting in an electron travelling in the acceptor phase of the active layer and a hole travelling in the donor phase. For this to occur successfully the low lifetime of an exciton in the donor materials necessitates a donor-acceptor boundary at which the exciton can be broken within approximately 10 nm. Furthermore, since the holes and electrons have to travel out of the active layer towards the electrodes, the domains of donor and acceptor needs to be connected in an interconnected network allowing both efficient dissociation of the excitons and efficient transport of the charge carriers to the respective electrodes. In this research used polymer with natural dye as active layer [35].

2.8 Photovoltaic Terminology

A PV or solar cell (used interchangeably) is the smallest production unit of PV systems and it is the building block of larger systems. Common single crystal silicon (a typical type of semiconductor material used) solar cells produce about 0.5 Volts. A group of cells wired together form a module. With single crystal silicon, 36 solar cells are often grouped together and wired in series to produce 18 Volts. A number of modules grouped together and attached to a mounting frame form a PV panel or solar panel. A group of panels make up a PV or solar array. There many different materials used for PV modules and different ways of configuring modules. Consequently, there are many different sizes (Watts) and voltages available in commercial modules. Effective PV system design allows the user to meet a wide variety of electrical loads.

2.9 PV System Components

A PV power system consists of several components, though the exact list may vary with the application. A remote water pumping system may utilize a DC water pump and be designed to operate only during the day when there is sun and the components may be the PV array (or panel or module depending on size of the load), a controller to regulate current and voltage, and the water pump, or load. A grid-tied system, like the one at your school, consists of the following components:

• PV array

• Inverter – converts DC electricity generated by the PV array to AC electricity fed into a building electrical panel (or sub-panel) (Note: a controller is built into the inverter)

• Emergency disconnects – allows for the PV array or the inverter to be disconnected

• DAS – Data Acquisition System – monitoring instruments (anemometer, temperature thermistor, pyrometer, and AC watt-hour meter) that display readings real-time on classroom computer PV systems that are designed to provide useful energy even when the sun is not shining will have two additional components – a battery bank that stores the excess electricity produced until it is needed and a charge controller that regulates the amount of current and voltage allowed to be fed into the battery bank[35].

2.10 Power Ratings of PV Modules

PV modules are tested and rated at Standard Test Conditions (STC) in a laboratory. NREL provides expert service to rate modules for a number of manufacturers. Standard Test Conditions include:

• Cell temperature of 25 °C

• Sun intensity of 1000 W/m2

• Spectral distribution at AM 1.5 (Air Mass 1.5)

Also, typically included in power ratings may be items such as the rated power of the module, current and voltage at typical load, short circuit current, open circuit voltage, and the dimensions of the module [35].

Chapter Three

Literature Review

3.1 Introduction

The energy problem encourages scientists to search for cheap efficient solar cells. One of most promising ones are Nano solar cells [36, 37, 38, 39, and 40].In this chapter one exhibit some of these all tempts [41, 42, and43].

3.2 Molecular doping of low –band gap - polymer: fullerene solar cells: Effects on transport and solar cells

This work is done by Ali VeyselTunc (Energy and Semiconductor Research Laboratory, In this work were separately dissolved in chlorobenzene, in concentrations of 1 mg/mL and 10 mg/mL, respectively. For the field-effect measure- ments, the dopant solution was added to the polymer solution to achieve concentrations of 0%; 0.1%; 0.2% and 0.3% by weight with respect to the polymer. Solutions were left stirring overnight. For the polymer: fullerene solutions, PCBM was added to obtain a weight ratio of 1:1 with respect to the polymer. The semiconducting layers were then spin coated onto pre-cleaned substrates. All solution processing was performed in a N2-filled glovebox. We show how molecular doping can be implemented to improve the performance of solution processed bulk heterojunction solar cells based on a low-bandgap polymer mixed with a fullerene derivative. The molecular dopant 2,3,5,6-tetrafluoro-7,7,8,8-tetracyanoquinodi methane (F4-TCNQ) is introduced into blends of poly[2,6(4,4-bis-(2-ethylhexyl)4H-cyclopenta[2,1-b:3,4-b0]-dithiophene)-alt-4,7-(2,1,3-benzothiadiazole)] (PCPDTBT) and [6,6]-phenyl-C61-butyric acid methyl ester (PCBM) via co-solution in a range of concentrations from 0% to 1%. We demonstrate that the hole conductivity and mobility increase with doping

concentration using field-effect measurements. Photoinduced absorption (PIA) spectroscopy reveals that the polaron density in the blends increases with doping. We show that the open circuit voltage and short circuit current of the corresponding solar cells can be improved by doping at 0.5%, resulting in improved power conversion efficiencies. The increase in performance is discussed in terms of trap filling due to the increased carrier density, and reduced recombination correlated to the improvement in mobility.We demonstrate that molecular doping using F4-TCNQ leads to an increase in the photocurrent in PCPDTBT:PCBMsolar cells. We investigate blends doped at 0; 0.1; 0.25, 0.5 and 1 wt.% with respect to the polymer. Field-effect measurements demonstrate that doping increases the hole conductivity and mobility in both PCPDTBT films and PCPDTBT:PCBM blends. The conductivity of the pristine polymer increases by more than ten times and for the polymer: fullerene blend by about four upon doping. The hole mobility was also observed to increase with doping concentrations between 0% and 0.3% by five times for the pure polymer and three for the blend. PIA spectroscopy revealed an increase in the polaron densities and a shift in the GSB band, corresponding to trap filling by the increase in charges introduced by doping. In solar cells, doping leads to increases in the photocurrent from 9.42 to 10.31 mA/ cm2 and an overall increase in the solar cell efficiency from 3.28% to 3.62 %. From the EQE data it is apparent that doping increases the efficiency in collecting photo generated charges in spectral regions attributed to the PCPDTBT absorption. These results show that molecular doping is a feasible and simple method to improve the efficiency of BHJ solar cells [41].

3.3 Electrochemically synthesized conducting polymeric materials for applications towards technology in electronics, optoelectronics and energy storage devices

This work was done by K. Gurunathan. The special emphasis is laid on the electrochemical synthesis of conducting polymers (CPs) including the choice of the monomers and solvents, supporting electrolytes and electrodes and structural aspects of these novel materials and the nature of the dopants which induce electrical conductivity in conjugated organic polymers .The electrochemical synthesis of novel electronic materials and their structure showed that besides the application oriented development and optimization, novel applications in more speculative ®elds such as polymer electronics or even molecular electronics may become feasible. Thus, applications of conducting polymers as photo conducting devices, solar energy conversion (PV) cells, in polymeric colored LEDs that could display images and form ¯at plastic screens for computers or TVs. They could also replace traditional LCDs, which are limited to a small size. Solid-state electro chromic cells for large area electro chromic devices (ECDs) are being used for commercial sign boards, time tables in airports and railway stations, calculators, clocks etc. In future, the world wide needs of economic fuel and pollution free environment can be met through the energy storage applications like rechargeable batteries and super-capacitors using conducting polymers as electrode material. These high-tech devices will be supercharge electronic products of the future. Some of the commercial products of conducting polymers. Worldwide several companies are racing to develop ultra-capacitors with millions of times the energy storage capacity of traditional capacitors. Ultra-capacitors store and release energy like batteries, but have vastly longer lives. They can unload their energy 10 to 100 times faster than batteries.

The new devices may lead to electric vehicles exhibiting superior performance of sports cars by releasingBursts of power when accelerating or climbing. Ultracapacitors are of great use in cellular phones and supercomputers. Most of the conducting polymers that have reached the actual application stage seem to be in a production test phase and are still waiting for a greater acceptance and utilization on the current market. Therefore, it is quite unclear at the moment how much pro®t is really made with devices basedon conducting polymers and whether the worldwide sales ®gure of synthetic metals which was forecast as 1 billion US$ in the year 2000 will be reached[42].

3.4 Enhanced electron injection in polymer light-emitting diodes: polyhedral oligomericsilsesquioxanes as dilute additives

This work was done by XiongGong . The molecular structures of MEH-PPV, MCC-POSS and MEH-PPV-POSS. The MEH-PPV and MEH-PPV-POSS were provided by Organic Vision (Canada). The synthesis of MEH-PPV-POSS was reported previously .The MCC-POSS was purchased from Hybrid Plastics. By blending monochlorocyclohexyl-polyhedral oligomericsilsesquioxanes (MCC-POSS)into poly(2-methoxy-5-(2'-ethyl-hexyloxy)-1.4-phenylenevinylene (MEH-PPV), enhanced luminous efficiency (LE, cdA−1) and brightness were observed in polymer light-emitting diodes (PLEDs) using Al as the Cathode. PLEDs made from MEH-PPV with 0.5 wt.% of MCC-POSS exhibit LE of 1 cdA−1, four times higher than that observed in simple MEH-PPV devices. X-ray diffraction studies, measurements of photovoltaic response and measurements of photoconductivity from the films of pure MEH-PPV and MEH-PPV with MCC-POSS demonstrated that the improved device performance results from mixing of MCC-POSS with MEH-PPV.

The enhanced electron-injection into the emissive layer results from the effect of the ionic conductivity introduced by the addition of MCC-POSS.In summary, we have demonstrated that improved luminous efficiencies can be achieved for PLEDs with Al as the cathode by blending the emissive conjugated polymer with polyhedral monochlorocyclohexyl- polyhedral oligomericsilsesquioxanes (MCC-POSS). XRD studies indicated that MCC-POSS are mixed with MEH-PPV, thereby affecting the morphology of MEH-PPV films and resulting in improved device performance. Additionally, the investigation of photovoltaic devices and steady-state photoconductivity from MEH-PPV and MEH-PPV with different concentrations of MCC-POSS demonstrated that the improvement in the device efficiency results from enhanced electron-injection associated with the ionic conductivity of MCC-POSS in the emissive layer [43].

3.5 Creation of a gradient polymer-fullerene interface in photovoltaic devices by thermally controlled inter diffusion

This work was done by M. Drees . Efficient polymer-fullerene photovoltaic devices require close proximity of the two materials toensure photo excited electron transfer from the semiconducting polymer to the fullerene acceptor. We describe studies in which a bilayer system consisting of spin-cast 2-methoxy-5-(28- ethylhexyloxy)-1,4-phenylenevinylene copolymer ~MEH-PPV! and sublimed C60 is heated above the MEH-PPV glass transition temperature in an inert environment, inducing an inter diffusion of the polymer and the fullerene layers. With this process, a controlled, bulk, gradient hetrojunction is created bringing the fullerene molecules within the exaction diffusion radius of the MEH-PPV throughout the film to achieve highly efficient charge separation.

The inter diffused devices show a dramatic decrease in photoluminescence and concomitant increase in short circuit currents, demonstrating the improved interface. © 2002 American Institute of Physics. @DOI: 10.1063/1.1522830# .In conclusion, we have fabricated polymer-fullerene bilayer systems in which the charge transfer and charge transport have been improved by thermally controlled inter diffusion. This leads to increased proximity of C60 molecules to optical excitations throughout the bulk of the film as demonstrated by luminescence quenching of one order of magnitude .The corresponding order of magnitude increase in photocurrent in the region of maximum absorption of the MEHPPV indicates the formation of a bulk hetrojunction due to thermally controlled inter diffusion. The optical absorption spectra of the MEH-PPV/C60 composite films before and after the inter diffusion process are indistinguishable, demonstrating that the enhanced photovoltaic efficiency is due solely to nanoscale control of the spatial locations of the two components [44].

3.6 Using Gum Arabic in Making Solar Cells by Thin Films Instead Of Polymers

In the work done by Abdelsakhi. 3 sample of Gum solar cells were made by depositing the Gum Arabic solution on ITO a glass by Spin Coating technical, and another layer was deposited from dye on a layer of Gum Arabic .Gold was fabricated on the layers to represent the anode and ITO Cathode. Gum Arabic based solar cells with Rhodamine 6G were fabricated on indium tin oxide by a spin coater position. Microstructure and cell performance of the solar cells with ITO/ Rhodamine 6G/ Gum Arabic structures were investigated. Photovoltaic devices based on the Rhodamine 6G / Gum Arabic hetrojunction structures provided photovoltaic properties under illumination. Absorption and energy gap

measurement of the Rhodamine 6G / Gum Arabic hetrojunction were studied by using UV-VS mini 1240 spectrophotometer and light current-voltage characteristics. The energy levels of the present solar cells were also discussed. The three ITO/Gum/Rhodamine/Au solar cells were produced and characterized, which provided efficiency (η) is (3.8 - 5.1 and 5.2) %. Fill factor (FF) is (0.964 - 0.9462 and 0.973), current density (Jsc) is (2.22 - 4.31 and 4.4) mAcm-2 and Open – circuit voltage (Voc) is (1.22 -1.25 and 1.209) V. This could be used at larger scale in promoting efficiency of solar cells. The application of conducting Arabic Gum to optoelectronic devices such as solar cell, light emitting diodes, and electrochemical sensors are of practical significance, because the Arabic Gum mixture can be easily prepared and modified by rich chemical procedures to meet optical and electronic requirements .This solar cell is cheap can be easily fabricated. It efficiency is relatively large [45].

3.7 Comparison of transparent conductive indium tin oxide, titanium-doped indium oxide, and fluorine-doped tin oxide films for dye-sensitized solar cell application

In the work done by Dong-JooKwak .the TCO materials investigated in this study are ITiO, ITO, and FTO. The FTO glass is commercially available from Pilkington Co., whereas the thin films of ITiO and ITO are prepared using RF magnetron sputtering. In this study, we investigate the photovoltaic performance of transparent conductive indium tin oxide (ITO), titanium-doped indium oxide (ITiO), and fluorine-doped tin oxide (FTO) films. ITO and ITiO films are prepared by radio frequency magnetron sputtering on soda-lime glass substrate at 300 °C, and the FTO film used is a commercial product. We measure the X-ray diffraction patterns, AFM micrographs, transmittance, sheet resistances after heat treatment, and transparentconductive characteristics of each film. The

value of electrical resistivity and optical transmittance of the ITiO films was 4.15×10-4 Ω-cm. The near-infrared ray transmittance of ITiO is the highest for wavelengths over 1,000 nm, which can increase dye sensitization compared to ITO and FTO. The photoconversion efficiency (η) of the dye-sensitized solar cell (DSC) sample using ITiO was 5.64%,whereas it was 2.73% and 6.47% for DSC samples with ITO and FTO, respectively, both at 100 mW/cm2 light intensity.In this study, we investigate the photovoltaic performance of transparent conductive ITiO, FTO, and ITO thin films. ITiO and ITO thin films are deposited on a soda-lime glass substrate by RF magnetron sputter method at relatively low substrate temperature (~300 °C) and at high rate (~10 nm/minutes), whereas the FTO film used is a commercial FTO glass. We investigate the electrical and optical properties of these films such as X-ray diffraction patterns, AFM micrographs, optical transmittance, sheet resistances, and photovoltaic characteristics. The near-IR transmittance of ITiO is the highest for wavelengths over 1,000 nm, which can increase dye sensitization in DSCs compared to ITO and FTO. The photo conversion efficiency (η) of the DSC sample using ITiO was 5.64%, whereas it was 2.73% and 6.47% from DSCs using ITO and FTO, respectively, both at 100 mW/cm2 light intensity [46].

3.8The Relationship between Energy Gab & Efficiency in Dye Solar Cells

In the work done by Sakina Ibrahim Ali. Four samples of (Ecrchrom Black T, DDTTC, Rohadamin B, Coumarin 500) solar cells were made by depositing the solution of Day sensitized on ITO Aluminum electrodes by Spin Coating technique and another layer was deposited from dye on a layer of (MEH-PPV).Al was used on the layers to act as anode and ITO as Cathode. A clean glass plate with a thin layer of ITO (Indium Tin

Oxide) was needed. The ITO acts as the first part of the solar cell, the first electrode. In this work dye sensitized solar cells made from: Ecrchrom Black T, DDTTC, RohadaminB,andCoumarin 500,with Al and TTO electrodes were fabricated. The energy gab of these dyes were found using UV Spectrometer. The energy gap for: Ecrchrom Black T, DDTTC, Rohadamin B, and Coumarin500 ; were found 2.16 eV ,2.20 eV ,3.27 eV and 3,60 respectively . The V- I characteristics for these cells and their performance were also found. The efficiency: Ecrchrom Black T, DDTTC, Rohadamin B, Coumarin 500 were found 1.66,1.62, 1.49 and 1.31. It is realized that; the efficiency increased when energy gab decreased. Ecrchrom Black T, DDTTC, Rohadamin B, Coumarin 500 were found 1.66,1.62, 1.49 and 1.31. It is realized that; the efficiency increased when energy gab decreased.

This work shows that the energy gap of the dyes used in dye sensitized solar cell affect the performance and efficiency of the solar cell [47].

3.9 Solar Storm Threat Analysis

This work was done by James A. Marusek. Most solar storms produce only minor disquieting affects on Earth. Typically one might expect short-term electrical power blackouts, short lived communication outages, rerouting of aircraft, loss of a few satellites and a beautiful “aurora borealis” in the nights sky from a large solar storm .But as the intensity of a solar storm increases like a wild beast, the storm can begin to develop the capacity to create a major disaster on Earth. The difference in solar storm intensity is like the difference between being hit with a tropical rainstorm and being devastated by a Category 5 hurricane. The solar storm of 1-2 September 1859, which began with a solar flare so strong that it was subsequently named the Carrington Flare, was such a beast. Oak Ridge National Laboratories estimated that only a solar storm just slightly stronger than the 13 March 1989 storm (Dst = 589 nT) would

have the capacity to produce a cascading blackout involving the entire Northeastern sector of the United States. So the question is “What damagewould a spawned geomagnetic storm like the one of 2 September 1859 (Dst = 1,760 nT) bring?” Would it simultaneously degrade and damage several unique large electrical transformers at key electrical generating stations taking down the massive power grid? Would the long lead-time required to manufacture and install replacement equipment result in major yearlong electrical blackouts, rolling blackouts and brownouts? How would a long-term lack of stable electricity affect advanced civilization? This work dissects and analyzes the various threats created by Great solar storms.

Most solar storms produce only minor disquieting affects on Earth. Typically one might expect short-term electrical power blackouts, short-lived communication outages, rerouting of aircraft, loss of a few satellites and a beautiful “aurora borealis” in the nights sky from a large solar storm. But as the intensity of a solar storm increases it develops the capacity to create a major disaster on Earth. A Great solar storm has the potential of seriously damaging the North American electrical power grid. The resulting blackout will be focused on the northern tier of states and the East and West coast of the U.S. and throughout Canada. The damaged equipment in the power infrastructure would generally have a replacement lead time of over a year due to its uniqueness. But the scope of the outage will be so great that governments will quickly elevate its repair to the level of a national imperative. As a result, restoration that might normally take over a year will occur in a matter of weeks. Critical elements affected by the blackout will include water, sewage, commerce, industry, banking, transportation, communications, and in the winter, heating. Because modern society relies so heavily on sophisticated technology, a long-term blackout will have a very profound effect on the

fabric of society. Many satellites will be destroyed or severely degraded. The loss will primarily target communications. The lead time to construct and replace these assets will be measured in terms of years [48].

3.10 Structure, properties and applications of fullerenes

This work was done by B.C. Yadav.This study reports about fullerenes, its structure, properties and applications. Fullerenes are the third allotropic form of carbon material after graphite and diamond. These were discovered in 1985 by Harold. W. Kroto, Robert F. Curl and Richard E. Smalley. Fullerenes consist of 20 hexagonal and 12 pentagonal rings as the basis of an icosahedral symmetry closed cage structure. Each carbon atom is bonded to three others and is sp2 hybridized .The C60 molecule has two bond lengths, the 6:6 ring bonds can be considered "double bonds" and are shorter than the 6:5 bonds. C60 is not "super aromatic" as it tends to avoid double bonds in the pentagonal rings, resulting in poor electron delocalization. As a result, C60 behaves like an electron deficient alkenes and reacts readily with electron rich species. The geodesic and electronic bonding factors in the structure account for the stability of the molecule. Fullerenes can be used as organic photovoltaic's (OPV), these are powerful antioxidants, reacting readily and at a high rate with free radicals which are often the cause of cell damage or death. Other uses of C60 like catalysts, in water purification and biohazard protection, portable power, Vehicles and medical.Thus this study gives the basic knowledge of structure of fullerenes and their applications. The fullerenes can be used as organic photovoltaic's (OPV). Other usesOf C60 like catalysts, in water purification and biohazard protection, portable power,Vehicles and medical [49].

3.11 Organic Semiconductor/Insulator Polymer Blends for High-Performance Organic Transistors

In the work done by Wi Hyoung Lee.In this study we reviewed recent advances in high-performance organic field-effect transistors (OFETs) based on organic semiconductor/insulator polymer blends .

Fundamental aspects of phase separation in binary blends are discussed with special attention to phase-separated microstructures. Strategies for constructing semiconductor, semiconductor/dielectric, or semiconductor/passivation layers in OFETs by blending organic semiconductors with an insulating polymer are discussed. Representative studies that utilized such blended films in the following categories are covered: vertical phase-separation, processing additives, embedded semiconductor nanowires.

We reviewed recent results with regard to organic semiconductor/insulator polymer blends for high-performance OFETs. The current pathway in the active layer was guaranteed by inducing vertical phase-separation, whereas a phase-separated insulator polymer could be used as a gate-dielectric or passivation layer. In contrast, an insulator polymer played a role as a processing additive for small molecular organic semiconductors. Embedded semiconductor nanowires are quite attractive for reducing semiconductor content and enhancing environmental stability, except for vertical phase-separation. Because phase separation is a complicated process that depends on molecular and processing parameters, appropriate selection of materials and processing conditions is essential for achieving high performance of organic semiconductor/insulator polymer blends [50].

3.12 Role of TiO2 Nanotube on Improvement of Performance of Hybrid Photovoltaic Devices

In the work done by SHI Quan-Min. The performance of TiO2 nanotubes in bulk hetrojunction of poly (2-methoxy-5-(2'-ethylhexyloxy)-1,4-phenylenevinylene) (MEH-PPV)/TiO2 nanotubes is investigated. The transport properties are studied byusing the time-of-flight technique (TOF). The carrier mobilities of both holes and electrons are not improved for the MEH-PPV:TiO2 composites compared with the pristine MEH-PPV. However, photoluminescence under the influence of the electric field indicates that the dissociation of exactions in the MEH-PPV:TiO2 composites, which is facilitated by photo induced charge transfer, only requires a smaller electric field.

In summary, the dissociation process and transport properties are investigated in MEH-PPV:TiO2 bulk hetrojunction . Compared to the pristine MEH-PPV, no transport improvement is observed for the MEH-PPV:TiO2 bulk hetrojunction. Charge transfer occurs at the TiO2 nanotube/polymer interfaces due to the PL quenching. However, the transfer efficiency for MEH-PPV/TiO2 interfaces is much lower than MEH-PPV/C60 interfaces. The dopant of TiO2 makes exaction dissociation more facilitated. The dissociation of exactions in the MEH-PPV:TiO2 composites only requires a smaller electric field. The improved performance of bulk-hetrojunction solar cells of MEH-PPV:TiO2 can be attributed to the facility of exaction dissociation at TiO2 interface.[51].

3.13 Non-linear I_V characteristics of MEH-PPV patterned on sub-micrometer electrodes

In this work done by J.H. Parka .The heavily doped Si substrate was thermally oxidized and was which spin-coated by an e-beam resistor

ŽPMMA. on the oxidized substrate. A sub-micrometer-wide line of a conjugated polymer MEH-PPV (2-methoxy-5-(2'-ethylhexyloxy)-1,4-phenylenevinylene).-p-phenylene vinylene .was patterned using a scanning electron microscope ŽSEM.. The spin-coated thin MEH-PPV film was exposed to the electron beam in SEM, resulting in an increase in cross-linking, which reduced the solubility of the MEH-PPV film. The polymer was developed in p-xylene to dissolve the non-irradiated part of the polymer. The width, length and thickness of the active patterned area, determined by the atomic force microscopy (AFM) image, was 500, 200 and 20 nm, respectively. The two-probe current voltage characteristics of the patterned MEH-PPV line were measured as a function of temperature. The higher field data of the non-linear I_V curves were fitted using the single carrier device model which considered the field and temperature dependent mobility with space charge limited conduction (SCLC). The estimated zero-field hole mobility was of the order of 10_3cm2/Vs with an activation energy of 0.038 eV. 2001 Elsevier Science B.V. All rights reserved.

This method of mask less patterning to make a sub micrometer-wide line of conjugated polymer MEH-PPV was done using SEM. The I_V characteristics of the patterned MEH-PPV line were measured as a function of temperature. Non-linear I_V curves were fitted in the high field region using a single carrier device model

developed by Blom et al ,which considers field dependent mobility with space charge limited conduction (SCLC). This gives a zero-field hole mobility μ E =0 of the order of 10_3 cm2/Vs and an activation energy D of 0.038 eV. As the temperature increases, the voltage gap of the I_V curves is decreased [52].

3.14 Charge Transport in Carbon Nanotubes-Polymer Composite Photovoltaic Cells

In the work done by AdnenLtaief. The MEH-PPV conjugated polymer and the SWNTs (Carbolex AP-grade, 12-15 angstrom diameter) were purchased from Aldrich. MEH-PPV has a molar mass of 86 000 g/mol determined by gel permeation chromatography (GPC). The ITO substrates were cleaned in an ultrasonic bath of acetone (HPLC grade) for 20 min, followed by isopropyl alcohol (IPA, HPLC grade) rinsing for 20 min at room temperature, before being dried in an nitrogen gas flow. MEH-PPV:SWNTs (1:1) composite solutions were prepared by blending the MEH-PPV with the SWNTs in an appropriate solvent, at a concentration of 15 mg/mL, and dispersing the SWNTs by using a magnetic stirrer. Sonication for 30 min is sufficient to give a stable transparent solution. In the first part of this work, the organic active layer of MEH-PPV or MEH-PPV: SWNTs (1:1) composite, is sandwiched between two electrodes on a glass substrate. The bottom electrode is an ITO layer, which serves as the anode and the top electrode is an Al layer, which is used as the cathode. In forward bias condition, the positive voltage was applied to the ITO layer with respect to the metal electrode. Photovoltaic cells were fabricated by spin coating (2,000 rpm for 20 s) the active bulk heterojunction layer onto a 100 nm precleaned ITO glasses of 1 cm × 1 cm coated with PEDFOT: PSS layer, using a “P6700 Series” spin coater. A layer of PEDOT: PSS between the transparent ITO electrode and the photoactive layer has been deposited from an aqueous solution onto the ITO substrate with an angular speed of 1,500 rpm. PEDOT: PSS films were dried on a hot plate under a nitrogen atmosphere for 10 min at 120 °C. Completion of the photovoltaic device occurs when aluminum contacts (typical thickness ~ 170 Å) are applied to the MEH-

PPV: SWNTs composite film layers. This is accomplished using thermal evaporation under vacuum at pressures <10-6 mbar with a standard shadow mask. The approximately thickness of the polymer/SWNTs layers was of the order of 500 nm. The effective solar cell area as defined by the geometrical overlap between the bottom ITO electrode and the top cathode was 0.1 cm2. The short circuit current and I-V curves were measured using a "Keithley 6430 SUB-FEMTOAMP REMOTE Source meter" source unit, using a Halogen lamp for illumination. Photovoltaic cell testing was performed in an isolated black box configuration to assure standard calibration and reproducibility of results. All processing steps were carried out in clean room conditions [36].

We have investigated the effect of SWNTs doping on the charge transport mechanisms of MEHPPV and MEH-PPV: SWNT (1:1) devices. Hopping of carriers between localized electronic states of the MEH-PPV polymer constitute the main mechanism for carrier transport. A clear link between the exponential distribution of the localized states and the observed power-law behavior of the only MEH-PPV device has been identified. The observed space-charge limited current (SCLC) regime of the photovoltaic cells is explained by an exponential tail state model for the polymer matrix, which is modified by the embedded SWNTs. The ability to construct organic D/A network composite photovoltaic cells containing single-walled carbon nanotubes (SWNTs)-polymer (MEH-PPV) composites has been demonstrated. The relatively high values of series and shunt resistances can be explained by a reduced photo generation rate and increased recombination rate, which is exacerbated by the proportional metallic nanotubes in the composite layers.

3.15Utilizing Carbon Nanotubes to Improve Efficiency of Organic Solar Cells

This work done by Richard Elkins. For our solar cells, where are used multi-walled carbon nanotubes as the electron donor and MEH-PPV-CN as electron acceptor. The CNTs were supplied by Zyvex and their diameter was 5-15 nm, their length was 0.5-5 μm, and were 60% metallic and 40% semiconducting. The CNTs were functionalized to improve their solubility.

In an effort to look at our project from a theoretical design standpoint we broke the current generation process down into four phases: photo generation of exactions, excitonic transport to the junctions, electron-hole separation, and charge transport to the electrode. The team looked at each of these steps from a conceptual and mathematical perspective and worked to develop a strong understanding of what steps (i.e. device thickness, material location/structure/concentration) we should take to optimize our device's output. It may turn out that one process is much slower than the others and the model for that "rate limiting step" becomes more important than the rest. However, we do not know if this is the case. In general, modeling bulk hetrojunction organic solar cells requires the use of extremely complex mathematical treatments that extend well beyond the capabilities of a one semester senior design project. Our approach to the problem must be simplified to focus on understanding the physics of polymer/nanotube solar cells on a basic level and applying this knowledge to our design. We will begin with a preliminary model of a simple bilayer hetrojunction, for which models can be developed, and we will extend the relevant results towards understanding the bulk hetrojunction [37].

The design of these components came from background knowledge that we spent a considerable amount of time collecting. Previous literature on the topic of organic solar cells provided helpful information and directions for our project. We looked to extend the well-studied trend of using C60 “Bucky” balls in the polymer to using carbon nanotubes. We developed a basic model that we felt would produce the best possible efficiency if we were able to place the materials in exact locations within the device. This model is simply a theoretical proposal; there is still work to be done mathematically and experimentally to verify if even our basic modeling assumptions were accurate. While we were designing an essentially optimal device, we were also working to create an operational device in the lab. Many devices were created using everything from pure polymer to pure nanotubes and many mixtures of the materials. While we were unable to produce a non-shorting device we feel reducing the concentration of nanotubes and restricting nanotube agglomeration will lead to fewer shorts. Overall, we were able to theoretically design a device, apply some of our theories within the lab, develop a recipe for fabrication, characterize a series of devices, and develop some theories for how we could improve the process in the future.

3.16The Change of Energy Gap and Efficiency of Carbon Solar Cell When Doped by Some Elements

This work is done by Mubarak DirarAbdalla,to study the change of energy gap and efficiency of carbon solar cell when doped by some elements. In this work six samples were prepared where C is doped with Zn, Mg, Al, S, Cd and Cu. The absorption, energy gap. When the carbon solar cell was doped with Mg, Al, S, Cu, Zn and Cd, the energy gap and efficiency changes. For Mg, Al, S, and Zn with atomic numbers Z: 12, 13, 16, and 30, the energy gap □□ increases and takes values 1.879,

1.897, 1.918, 1.925 eV respectively. This may be related to the fact that, according to hydrogen like atoms, the energy gap increases with atomic number. However the efficiency decreases for this group to be 0.780, 0.730, and 0.023 for Al, S, and Zn respectively. This is since the increase of energy gap decreases the number of electron that reaches conduction band, which in turn decreases efficiency. For Cu and Cd with Z= 29 and 48 decreases to be 5.184 and5.107 respectively. This is related to the inverse effect of atomic radius on, where r increases with Z. The efficiency increases as decreases.

The results show that the efficiency and energy gap of carbon solar cell is affected by the atomic number. This raises a hope in increasing efficiency by doping solar cells with impurities [38].

3.17 Determination of Energy Gaps and Effect of Temperature on the Absorption and Transmittance Spectrum on Photoelectrodye

The work done by Asim Ahmed Mohamed Fadoll , is concerned with determination of energy gaps and effect of temperature on the absorption and transmittance spectrum on photoelectron dye. In this work a sample of fresh Roselle was making .The optical properties of the dye Roselle anthocyanin's shows high absorption to visible spectrum because of concentration of anthocyanin in Roselle calyces. Its absorption to sun light is almost constant which an indication of chemical stability. The absorption spectrum of the anthocyanin dye dissolved in methanol shows λ_{max}v(283 nm) in the UV region, while λ_{max} (545 nm) in the VIS range. The corresponding energy levels are 4.36 eV and 2.25 respectively .The absorption spectrum of fresh Roselle crude shows in the visible region. The energy gap of Roselle is 2.06, while that of titanium dioxide is 4.125. These values agree with the standard values. The responseof optical

absorption to temperature shows stability at ambient temperature, while absorptiondecreases as temperature increases above ambient temperature.The results obtained show that the thermal properties of the Roselle anthocyanin dye indicates that its absorption property, i.e., the ability of atoms to trap visible photons, is stable and does not affected by temperature at ordinary ambient temperature. But at higher temperatures the absorption decreases. It shows also almost temperature absorption to direct sun light thus indicates high chemical stability. The optical property of the Roselle anthocyanin dye shows high efficiency to absorb visible light. This may have a direct impact on increasing the efficiency of the solar cell, as for as the function of the dyes to trap visible light [39].

3.18 Optical Properties of Glass and Plastic Doped by CU

In the work done by Elharam Ali Eltahir Mohammed, Five samples plastics and glasses were doped by Cu with different concentration ranging from 28.9 mg/cm^2 to 1965.8□g/cm2. The optical properties of samples were studied by using the following devices with the following specification. Glass and plastic samples are doped with Cu at different concentrations. The results obtained show that increasing Cu concentration decreases absorption coefficient, refractive index, real and imaginary electric permittivity, whereas energy gap increases. These results surprisingly agree with the theoretical model that treats Cu as an electric dipole.

The results show that absorption of light by glass can be changed by changing the concentration of Cu. The increase of Cu concentration decrease absorption coefficient. This means that in the design of windows in homes one can enable more light to pass into the room, by decreasing concentration of Cu. It can be also be used in designing sensor and solar cells to improve their performance [40].

3.19 Optical and Electrical Characteristics of TIO2 – MEH Multilayers Thin Film

In this work done by TayiserMohiEldinElmahdi, The organic compounds MEH-PPV and TiO2 were used study to construct four samples which are multi-layers structures to study their optical and electrical characteristics. The optical and electrical properties of TiO2-MEH-PPV double layer were studied when their number is increased. It was found that increasing the number of double layers decreases the energy gap which may result from the effect of the internal MEH electric field that allows some energy levels to enter the energy gap. The absorption also increases when layers were increased which may result from the narrowing of the energy gap. The current however decreases up on increasing the layers which may be related to the increase of electric resistance.The results show that the energy gap of TiO2 - MEH double layer can be decreased and the absorption can be increased by increasing the number of them. Thus increase of TiO2 - MEH layers decreases current [41]

3.20Energy Gaps, Donor and Accepter Levels for Polymer Solar Cells Doped with Different Dyes

In the work done by EnamIzeldin Ibrahim Elsayd. The energy levels and energy gaps of polymer solar cells values were found when they are doped with Coumarin, Lawsonia, Rohdamin B, Blue 8GX, Roselle, DDTTC and Ero-Chrom black, by means of the values of absorption and transmission spectra, beside values of absorption coefficient- intensity relations of them. The results obtained for shows that the absorption spectra which relates intensity and emitted wave lengths for them gives the values of donor and acceptor levels which are 5.07 , 4.41 , 5.08, 5.12 ,4.57, 4.88, 5.54eV respectively 2.43, 2.25, 2.45, 2.84, 2.32 , 2.41 2.33eV respectively. The transmission spectra for Coumarin, Lawsonia,

Rohdamin B, Blue 8GX, Roselle, DDTTC and Ero-Chrom black is closely related to their energy gaps which were found to be 1.17, 3.58, 1.10, 1.08, 3.06, 1.52, 1.11 eV these values are in conformity with the results obtained by the absorption coefficient - intensity relations which predicts the energy gaps 3.55, 3.30, 3.27, 3.15, 3.08, 2.94eV and 2.59eV which are in agreement with the standard values. The results show that the application of conducting polymers to optoelectronic devices such as solar cell. Dyes Structure showed high optical absorption in the range of (200 to 537) nm. To increase power conversion efficiency, structures of the solar cells should be optimized[42]

3.21 Performance improvement of MEH-PPV: PCBM Solar Cells Using Bathocuproine and Bathophenanthroline as the Buffer Layers

In the work done by L.X. Dphg all the devices in this work were fabricated on indium tin oxide (ITO)-coated glass substrates, which had been carefully cleaned by acetone, ethanol and de-ionized water consecutively, and finally dried by blowing with nitrogen gas and baking at 80 ◦C for 5 min in air. After the dried ITO glass substrates were treated by UV ozone for 10 min, the filtered poly(3,4-ethylenedioxythiophene):poly(styrenesulfonate) (PE- DOT:PSS) was spin coated on the top of the ITO surface with a speed of 2000 rpm (round per minute) for 50 s and then annealed in a vacuum at 120 ◦C for 10 min. The MEH-PPV: PCBM, dissolved in chlorobenzene with a weight ratio of 1:4, was spin coated onto the PEDOT: PSS layer at the same speed of 2000 rpm. Layers of Bphen, BCP, LiF and an aluminum (Al) electrode were thermally evaporated un- der high vacuum. Deposition rates were monitored with a quartz oscillating crystal and controlled to be 1 ˚A/s for both organic layers and LiF. A shadow mask was used for the deposition

of the cathode, giving an active device area of 0.1 cm^2. The de- vice configuration of organic photovoltaic cells used in the study.We investigated the effects of interfacial buffer layers—BCP and Bphen on the performance of polymer solar cells based on MEH-PPV and PCBM blend. After inserting 5-nm BCP and 12-nm Bphen between the active layer and the cathode, the PCE are substantially increased by a factor of 0.69 and 1.16, respectively, as compared with the devices without any buffer layer. The roles of BCP and Bphen might be the same for efficiency improvement because of their similar optical transparency and energy gap. How- ever, compared with traditional devices by using LiF as the buffer layer, the BCP-based devices show a com- parable efficiency, while Bphen-based devices show a much higher efficiency. This is due to the better electron transport ability of Bphen than that of BCP [44].

3.22Non-linear I–V Characteristics of MEH-PPV Patterned on Sub-micrometer Electrodes

In the work done by J.H. Parka, the heavily doped Si substrate was thermally oxidized and was spin-coated by an e-beam resistor ŽPMMA. On the oxidized substrate. We drew the electrode pattern directly using an e-beam lithography ma- chine. After development, a negative PMMA pattern remained. A NiCr alloy was deposited to improve adhesion to the substrate before a thick Pt layer was de- posited, which was evaporated by e-gun. At the lift-off process, we removed all of the negative PMMA pattern in the acetone. In this way, a Pt electrode on the oxidized substrate was fabricated. MEH-PPV dissolved in *p*-xylene was spin-coated onto the Pt electrode. We drew the e-beam line across the Pt electrode using a SEM. The solubility of the polymer was affected by the high energy electrons. The polymer was developed in *p*-xylene to

dissolve unexposed polymer ŽFigs. 1 and 2 The MEH-PPV patterned electrode was attached to a chip carrier by silver paste. The electrode and external probes were connected by wire bonder. The sub- micrometer-sized device of the un doped polymeric semiconductor was measured at various temperatures using a cryostat in a vacuum. Constant voltage was supplied by Keithley 6517A and the resulting current was measured by another Keithley 6517A. The noise level during the *I–V* measurements was a few pA while the signal level was nA. Because the resistivity of the sample was so high and the RC response time was so long, we took the data after the signal was stabilized.

This method of mask less patterning to make a sub- micrometer-wide line of conjugated polymer MEH-PPV was done using SEM. The *I–V* characteristics of the patterned MEH-PPV line were measured as a function of temperature. Non-linear *I–V* curves were fitted in the high field region using a single carrier [45].

3.23 Comparison of Transparent Conductive Indium Tin oxide, Titanium-doped Indium oxide, and Fluorine-doped Tin oxide Films for Dye-sensitized Solar Cell Application

In the work done by Dong-JooKwak , the TCO materials investigated in this study are ITiO, ITO, and FTO. The FTO glass is commercially available from Pilkington Co., whereas the thin films of ITiO and ITO are prepared using RF magnetron sputtering. In this study, we investigate the photovoltaic performance of transparent conductive indium tin oxide (ITO), titanium-doped indium oxide (ITiO), and fluorine-doped tin oxide (FTO) films. ITO and ITiO films are prepared by radio frequency magnetron sputtering on soda-lime glass substrate at 300 °C, and the FTO film used is a commercial product. We measure the X-ray diffraction patterns, AFM micrographs, transmittance, sheet resistances after heat

treatment, and transparent conductive characteristics of each film. The value of electrical resistivity and optical transmittance of the ITiO films was 4.15×10-4 Ω-cm. The near-infrared ray transmittance of ITiO is the highest for wave lengths over 1,000 nm, which can increase dye sensitization compared to ITO and FTO. The photo conversion efficiency (η) of the dye-sensitized solar cell (DSC) sample using ITiO was 5.64%, whereas it was 2.73% and 6.47% for DSC samples with ITO and FTO, respectively, both at 100mW/cm^2 light intensity.

In this study, we investigate the photovoltaic performance of transparent conductive ITiO, FTO, and ITO thin films. ITiO and ITO thin films are deposited on a soda-lime glass substrate by RF magnetron sputter method at relatively low substrate temperature (~300 °C) and at high rate (~10 nm/minutes), whereas the FTO film used is a commercial FTO glass. We investigate the electrical and optical properties of these films such as X-ray diffraction patterns, AFM micrographs, optical transmittance, sheet resistances, and photovoltaic characteristics. The near-IR transmittance of ITiO is the highest for wavelengths over1,000 nm, which can increase dye sensitization in DSCs compared to ITO and FTO. The photo conversion efficiency (η) of the DSC sample using ITiO was 5.64%, whereas it was 2.73% and 6.47% from DSCs using ITO and FTO, respectively, both at 100 mW/cm2 light intensity [46].

3.24The Relationship between Energy Gab & Efficiency in Dye Solar Cells

In the work is done by Sakina Ibrahim Ali. Four samples of (Ecrchrom Black T, DDTTC, Rohadamin B, Coumarin 500) solar cells were madeby depositing the solution of Day sensitized on ITO Aluminum electrodes by Spin Coatingtechnique and another layer was deposited from dye on a layer of (MEH-PPV).Al was used on the layers to act as anode and ITO

as Cathode. A clean glass plate with a thin layer of ITO (Indium Tin Oxide) was needed. The ITO acts as the first part of the solar cell, the first electrode. In this work dye sensitized solar cells made from: Ecrchrom Black T, DDTTC, Rohadamin B, and Coumarin 500, with Al and TTO electrodes were fabricated. The energy gab of these dyes were found using UV Spectrometer. The energy gap for: Ecrchrom Black T, DDTTC, Rohadamin B, and Coumarin500 ; were found 2.16 eV ,2.20 eV ,3.27 eV and 3,60 respectively . The V- I characteristics for these cells and their performance were also found. The efficiency: Ecrchrom Black T, DDTTC, Rohadamin B, Coumarin 500 were found 1.66, 1.62, 1.49 and 1.31. It is realized that; the efficiency increased when energy gab decreased .Ecrchrom Black T, DDTTC, Rohadamin B, Coumarin 500 were found 1.66,1.62, 1.49 and 1.31. It is realized that; the efficiency increased when energy gab decreased.

This work shows that the energy gap of the dyes used in dye sensitized solar cell affect the performance and efficiency of the solar cell [47**].**

3.25 International Journal OF Engineering Science & Research Technology

In the work is done by Sakina Ibrahim Ali. Six samples were prepared by depositing HEH-PPVand using a different electrode Al, Agand Auto act as an anode were prepared. The V- I curve for all solar cell sample were found by using electric circuit consisting of ammeter, volt meter and power supply. In this work the effect of changing the anode of polymer solar cell on their performance was experimentally investigated .The cells were fabricated from ITO which act as a cathode beside MEH PPV, Ecrchrom Black T and Rohadamin B dyer. The anodes which care Al, Ag, Au with atomic number 13, 47 and 79 were used. It was found that the efficiency of the solar cell of Al, Ag, Au electrode for Ecrchrom dye

are 1.66, 1.59, and 1.58Respectively the efficiency for Rohadamin ,Ecrchrom Black T dye are 1.49, 1.48 and 1.46 respectively these results shows clearly that the efficiency increases as the atomic number decreases this conforms with the fact that energy gap increase with the atomic number. This work shows that the electrode type affect polymer solar cell performance. This performance depend on the atomic number of the electrode [48**]**

3.26 First-principles investigation of the optical properties of crystalline poly(di-n-hexylsilane)

This work is done by W. Y. Ching .He used the orthogonalized linear combination of atomic orbital's (OLCA) method to calculate the electronic structure of the Pdn6s crystal. This is an all-electron fully self-consistent method based on the LDA of the density functional theory (DFT), and is known for its efficiency and accuracy especially for complex crystals. The optical properties of poly(di-*n*-hexylsilane) are studied by first-principles local-density calculations based on the crystal structure recently determined by x-ray diffraction. The one-dimensional nature of the band, the orbital composition of the states, and the charge distribution of the highest- occupied –molecular –orbitals lowestunoccupied –molecular-orbitals states on the Si backbone, the effective masses, and the anisotropic optical conductivity are all clearly delineated. (S0163-1829~96!04543-2).

In conclusion, the LDA-based first-principles band approach is very effective in elucidating the structure and properties of the polysilane polymers. The present calculation delineates the nature of bonding in one such polymer and unequivocally show that optical properties in the UV region are mainly controlled by the orbital bonding of the Si backbone. It is thus expected that different backbone confirmation

can change the HOMO and LUMO state levels and wave functions to give different optical spectra. This is consistent with the notion that thermo chromium in Pdn6s is associated with an order-disorder transition from an all-transto a one at least partly *trans-gauche*, with the accompanied variations in the structural arrangements of the side chains. This certainly affects the formation of bond exciton below the CB edge. The present calculation also demonstrates for that the Si 3*d* orbitals are important in the unoccupied states which determine the optical properties in the UV region [49].

3.27 Electrical and Optical Properties of Fluorine Doped Tin Oxide Thin Films Prepared by Magnetron Sputtering

This work is done by Ziad Y. Banyamin .In this work FTO thin films were deposited onto standard size (5 mm by 25 mm, 1 mm thick) microscope glass slides using a mid-frequency pulsed DC magnetron sputtering technique from loose powder targets. Different fluorine doping levels were prepared in the tin oxide powder targets in order to study the effect of doping level on the structure and photoelectrical properties of the thin films. Fluorine doped tin oxide (FTO) coatings have been prepared using the mid-frequency pulsed DC closed field unbalanced magnetron sputtering technique in an Ar/O2 atmosphere using blends of tin oxide and tin fluoride powder formed into targets. FTO coatings were deposited with a thickness of 400 nm on glass substrates. No post-deposition annealing treatments were carried out. The effects of the chemical composition on the structural (phase, grain size), optical (transmission, optical band-gap) and electrical (resistivity, charge carrier, mobility) properties of the thin films were investigated. Depositing FTO by magnetron sputtering is an environmentally friendly technique and the use of loosely packed blended powder targets gives an efficient means of

screening candidate compositions, which also provides a low cost operation. The best film characteristics were achieved using a mass ratio of 12% SnF2 to 88% SnO2 in the target. The thin film produced was polycrystalline with a tetragonal crystal structure. The optimized conditions resulted in a thin film with average visible transmittance of 83% and optical band-gap of 3.80 eV, resistivity of $6.71 \times 10^{-3}\Omega\cdot$cm, a carrier concentration (Nd) of 1.46×1020 cm^{-3} and a mobility of 15 cm^2/Vs.

Transparent conductive oxide SnO2:F thin films have been deposited on glass substrates by the pulsed DC magnetron sputtering technique in an Ar/O2 atmosphere using loosely packed blended powder targets. The thin films were grown at a deposition rate of 27 $nm\cdot min^{-1}$ and a deposition temperature below170 °C. It was determined that 5.3 at.% of fluorine incorporated into the film gave the best electrical behavior. In addition, the XRD structural analysis showed that the crystallinity of the SnO_2 samples were improved with the fluorine incorporation and the intensity of the (200) plane ameliorated with the increase in the fluorine concentration up to 5.3 at.% found in the thin film. The average optical transmittance achieved for this coating was 83% across a range of $300 \leq\lambda\leq 900$ nm. The detailed analysis of the electrical properties of the thin film as a function of the fluorine doping level revealed that a resistivity as low as$6.71 \times 10^{-3}\Omega\cdot$cm was obtained with a fluorine content of 5.3 at.%.This work has shown the ability to grow transparent conductive oxide $SnO_{2:}$ F thin films using a cost effective (no post annealing of samples, and high deposition rate) and environmentally friendly method(no fluorine gas is used and no toxic affluent is produced). This technique is of great advantage for studying the properties of multi component materials and identifying optimum compositions [51**].**

3.28 Applications of Oxide Coatings in Photovoltaic Devices

This work is done by Sonya Calnan. Metalloid and metal based oxides are an almost unavoidable component in the majority of solar cell technologies used at the time of writing this review. Numerous studies have shown increases of ≥1% absolute in solar cell efficiency by simply substituting a given layer in the material stack with an oxide. Depending on the stoichiometry and whether other elements are present, oxides can be used for the purpose of light management, passivation of electrical defects, photo-carrier generation, charge separation, and charge transport in a solar cell. In this review, the most commonly used oxides whose benefits for solar cells have been proven both in a laboratory and industrial environment are discussed. Additionally, developing trends in the use of oxides, as well as newer oxide materials, and deposition technologies for solar cells are reported.

Oxides are an important component of PV cells and shall continue to be so in the future. Due to the diverse applications of oxides in PV cells, only a snap shot can be made of the range of devices that have been explored. On the one hand, we have the traditional oxides for various functionalities and on the other, new oxide materials are being introduced for use in PV. While the transparent conducting oxides of indium, zinc and tin are important as electrodes in most PV cell technologies, TiO_2 has become the model material for PV cells based on charge transfer to a sensitized semiconductor. The oxides of silicon and aluminum, both members of the semi-metal group, when highly insulating can be used for passivation due to their high dielectric constant. The transition metal oxides with high work functions are now routinely used for organic PV cells as electrode buffer materials to maximize the cell voltage and to prevent leakage currents. Other oxides, such as those of copper and lead have been used as absorber materials. More exotic multiparty oxides such as the ferroelectric Perovskite $BiFeO_3$ and $KNbO_3$ are used as absorbers

with the promise of high cell voltage. Lanthanide host oxides and lanthanide doped oxides have been introduced as wide band spectral converters to enhance the spectral response of PV cells beyond the normal absorption band of the absorber material. Much as this review has focused on examples of applications of oxide materials where PV cell performance has been experimentally demonstrated, the contribution and importance of theoretical calculations towards these and future developments cannot be overstated [52].

3.29 The Effect of Different Dyes on the Efficiency of Polymer Solar Cell

This work is done by Omer Abdalla Omer Gassim. In this work polymer cells with different thicknesses and three different type of organic dyes (Rhodamine 6G, Coumarin 500 and Dibenzocyanin 45) are used in fabrication. The effect of the concentration of different organic dye on various electrical and optical properties of the samples produced has been studied. It was found that when the conjugate polymer layer deposition on the slides at low speeds by spin coating technique (increasing the thickness of the conjugate polymer layer), results gave a recognized higher efficiency in the tested cell. The use of the organic dye (DDTTCI) led to improve in efficiency and absorption coefficient of light in the samples used. In addition, the optical absorption spectra were recorded for those samples with a UV -VIS spectrophotometer (model: UV mini-1240) within the wavelength range of 200–800 nm, at room temperature. The samples show variations in absorption coefficient directly depending on the type of organic dye used as well as the concentration of conjugate polymer. The short-circuit current, open circuit voltage and the fill factor of each sample have been calculated. The efficiency was found in the range of 10.28-1.744% for

designed samples.In this work calculations of IV Characterization and absorbance spectra of conjugated polymers have been made and different types of polymer solar cells have been produced. Five samples of solar cells have been fabricated. The optical absorbance of these films was measured by UV-VIS spectrophotometer. The samples show a wide range of absorption of the solar spectrum. Sample A5 and sample A2 was recorded the highest absorbance and the lowest absorbance, respectively. For the IV -curve obtained for the conjugate polymer solar cells a curve similar to the curve from the optimal model as described in (I. Montanari, 2002). All samples showed a variation in terms of obtained efficiency ranged between 10.28 % - 3.117 %[53].

3.30 The Effect of Exchanging the ZnO and CnO Layers on Their Performance

This work done by ThowraAbdElradiDaldowm. In this work two solar cell types were fabricated. The first type is FTO/ CuO/ ZnO/ Al and the second type is FTO/ ZnO/ CuO/ Al. Six samples were prepared from each type. The efficiency for each type was obtained. It was found that the efficiency of FTO/ ZnO/ CuO/ Al is in the range ~ 0.6×10^{-3} , while the efficiency of FTO/ CuO/ ZnO/ Al is in the range ~ 2×10^{-3}. The difference may be attributed to the fact that FTO and CnO acts as p - type semiconductor, while ZnO act an n- type semiconductor. Thus the first type acts as pnp component thus have low efficiency, while the second type acts ppn component and have relatively high efficiency

The results show that the solar cell which is formed from FTO/ CuO/ ZnO/ Al respectively is more efficient and has good performance compared to FTO/ ZnO/ CuO/ Al solar

cell. The efficiency can be increased considerably by adding donors to ZnO and acceptors to CuO [54].

3.31 Optical Properties of Glass and Plastic Doped by CU

In the work is done by Elharam Ali Eltahir Mohammed, Glass and plastic samples are doped with Cu at different concentrations. The results obtained show that increasing Cu concentration decreases absorption coefficient, refractive index, real and imaginary electric permittivity, whereas energy gap increases. These results surprisingly agree with the theoretical model that treats Cu as an electric dipole.The results show that the absorption of light by glass can be changed by changing the concentration of Cu. The increase of Cu concentration decrease absorption coefficient. This means that in the design of windows in homes one can enable more light to pass into the room, by decreasing concentration of Cu. It can be also be used in designing sensor and solar cells to improve their performance [55].

3.32 Optical and Electrical Characteristics of TIO2 – MEH Multilayers Thin Film

This work is done by TayiserMohiEldinElmahdi. The optical and electrical properties of TiO2-MEH-PPV double layer were studied when their number is increased. It was found that increasing the number of double layers decreases the energy gap which may result from the effect of the internal MEH electric field that allows some energy levels to enter the energy gap. The absorption also increases when layers were increased which may result from the narrowing of the energy gap. The current however decreases up on increasing the layers which may be related to the increase of electric resistance.The results show that the energy gap of TiO2 - MEH double layer can be decreased and the absorption can be increased by increasing the number of them. Thus increase of TiO2 - MEH layers decreases current [56].

Chapter Four

Experimental, Results and Discussion

4.1 Experimental

4.1.1 Introduction

This chapter is concerned with the experimental work. This includes sample preparation, apparatus, theory and the experimental work set up. In this work solar cell types with different dyes were fabricated.

4.1.2 The Materials of an Organic Solar Cell

4.1.3 ITO

ITO (Indium Tin Oxide) is a transparent conductive material. It is a mixture of indium oxide (In2O3) and tin oxide (SnO2). ITO is used as one of the electrodes in the solar cell .ITO can absorb light at the same wavelength as MEH-PPV. This is important because only the light absorbed by MEHPPV may result excitations[61].

4.1.4Rhodamine B

Constitution 2-[6-(Diethylamino)-3-(diethylimino)-3H-xanthen-9-yl] benzoic acid Rhodamine 610 - $C_{28}H_{31}N_2O_3Cl$ · MW: 479.02

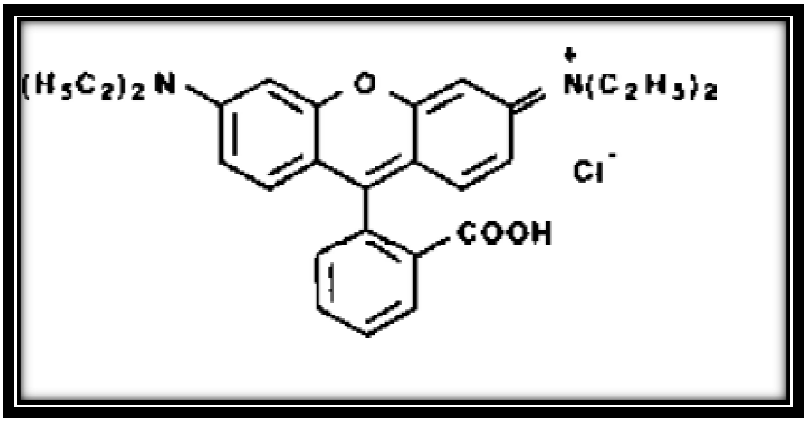

Fig (4.1) Rhodamine B

Characteristics Lambdachrome® number: 6100 CAS registry number: 81-88-9Appearance: green, crystalline solid Absorption maximum (in ethanol): 552 nm Molar absorptivity: 10.7 x 10^4 L mol^{-1} cm^{-1} Fluorescence maximum (in ethanol):580 nm for research and development purposes only [62].

4.1.5 TiO_2

Titanium dioxide (TiO2) is one of the most effective photocatalysts currently in use due to its strong oxidizing power, non-toxicity and long-term physical and chemical stability. It has been widely used for the decomposition of organic compounds and microbial organisms, such as cancer cells, viruses and bacteria as well as its potential application in sterilization of medical devices and air-conditioning filters owing to its self-sterilizing property [4–7]. When irradiated with near UV light, TiO2 exhibits strong bactericidal activity [8]. The photogenerated holes and electrons react with water and oxygen respectively to form hydroxyl radicals (·OH) and other reactive oxygen species, such as singlet oxygen (O^{-2}), and hydrogen peroxide (H2O2) [9]. Thus, TiO2 and TiO2 deposited materials could kill bacteria and also simultaneously degrade the toxic compounds exhausted from the bacteria [7]. Complete oxidation of organic compounds and the whole cells to carbon dioxide can be achieved [10]. However, its drawbacks of the low quantum yields and the lack of visible-light utilization hinder its practical application. To overcome these problems, numerous studies have recently been performed to enhance the photocatalytic efficiency and antibacterial activities, such as doping noble metals [11–14]. It is reported [15–17] that loading of silver nanoparticles highly enhances the photocatalytic activity of TiO2. The enhancement is attributed to its ability to trap electrons at Schottky barriers at each Ag–TiO2 contact region, which reduces the recombination of light generated e−–h+ at the TiO2 surface.

Therefore charge separation is promoted and more electron transfer occurs, and consequent longer electron–hole pair lifetimes.

4.1. 6 Zinc oxide (ZnO)

The emphasize here will be on the fundamental properties of ZnO, like growth, electrical and optical properties, since the potential for optoelectronic devices based on ZnO is also one of the main motivations for the present work. ZnO is a direct wide band-gap (3.37 eV at room temperature) II-VI binary compound semiconductor and crystallizes in three forms: hexagonal wurtzite, cubic zincblende, and the rarely observedcubic rocksalt [11]. The hexagonal wurtzite structure of ZnO is the mostcommon phase having a crystal structure C6v or P63mc, which occursalmost exclusively at ambient conditions [12, 13]. The wurtziteZnOstructure consists of alternating zinc (Zn) and oxygen (O) atoms is shownin fig (4.2) . The ZnO structure has polar surface (0001) which is eitherZn or O terminated and non-polar surfaces (1120) and (1010) possessingan equal number of both atoms. The polar surface of ZnO is highly metastablein nature and is responsible for several unique and astonishingproperties including piezoelectric properties, it also play a key role incolumn growth, favorable for etching due to higher energy. The polarsurface is also known to possess different physical and chemical properties[14].

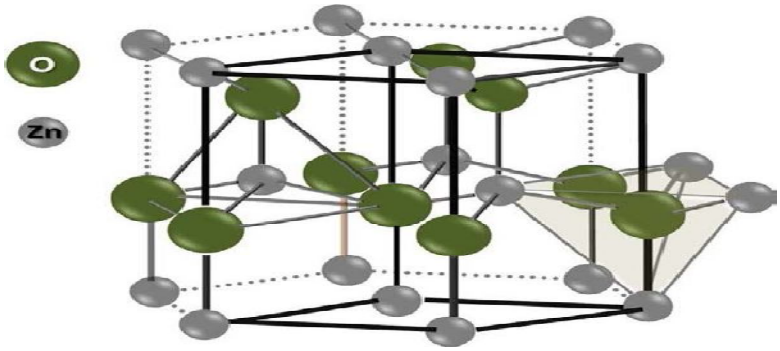

Fig(4.2)Crystal structure of hexagonal wurtziteZnO.

4.2Methods

Ten sample of solar cells were made by tow group of material used one isTiO_2 and other is ZnO and doping by five oxide (Mg O, CoO, CdO, Li_2O and Al_2O_3) .Gold(Au) was fabricated on the layers to acts anode and ITO Cathode. A clean glass plate with a thin layer of ITO (Indium Tin Oxide) is needed. The ITO acts as the first part of the solar cell, the first electrode. However a bit of the ITO has to be removed, to avoid short-circuiting For the purpose of the present study Day sensitized devices were made following the generally accepted methods. The fabrication process started by preparing (TiO_2 ,ZnO ,Mg O, CoO, CdO, Li_2O and Al_2O_3) material. Gold(Au) electrode was used to complete the formation of solar cell. The formed (TiO_2 ,ZnO ,Mg O, CoO, CdO, Li_2O and Al_2O_3) were characterized by Ultra violet-visible spectroscopy. Electrical circuit containing the (voltmeter and Ammeter and a light source Lamp with the intensity radiological" and a solar cell) were characterized the solar cells. The solar cell was exposed to light and the current and voltages of the cell recorded.For the purpose of the present study solar cells devices were made following the generally accepted methods. The (TiO_2 , ZnO ,Mg O, CoO, CdO, Li_2O and Al_2O_3) material was made firstly by chemical method (148.74 g of Ti($NO_3)_2 3.H_2O$, 14.542 g of Zn($NO_3)_2 6H_2O$,3.929 g of Mg ($NO_3)_2 6H_2O$, 4.614 g of

Co($NO_3)_2 6H_2O$, 5.803 g of Cd($NO_3)_2 6H_2O$,7.29 g of ($NO_3)_2 6H_2O$ Li_2O and 6.19 g of Al_2($NO_3)_3 6H_2O$) all was dissolved (11.2 ml of deionize water)to made five oxide (Mg O, CoO, CdO, Li_2O and Al_2O_3).Been made TiO_2 and other is ZnO and doping by five oxide (Mg O, CoO, CdO, Li_2O and Al_2O_3) .

4.3 Apparatus:

10 type of solar cell (2.5×2.5) cm with two group of material used one isTiO_2 and other is ZnOthey are doped by five oxide (Mg O, CoO, CdO, Li_2O and Al_2O_3) ,Rhodamine B chemical dyes was used , 1 microvolt-DMM- voltmeter, KETHLEY-USA- 177 DC,1electrometer-ammeter, KETHLEY-USA- 642 DC, 1 halogen lamp housing, 12 V, 50/100 W 450 64 , rjoostat -Albert van der perk nV Rollerdom-No-464151-27Ω-5.2A, light OF intensity (scouts light, power of 0.55W.cm^{-2}),Connecting wires.The purpose of this experiment is to find out the fill factor and efficiency of polymer solar cell by using ten samples. Measures absorbance, emission and permeability.

Fig (4.3) UV spectrometer device

4.4Experimental Setup:

- Each solar cell is connected such that the upper negative pole to the lower positive pole were connected using two bridging plugs (series connection of four solar cells).
- The STE potentiometer as a variable resistor was connected it to the solar battery using bridging plugs.
- The ammeter was connected in series with the solar battery and the variable resistor. The measuring range was selected to be 100 10^{-11}A DC.
- The micro voltmeter was connected in parallel to the solar cell.
- The scouts light lamp was connected to the transformer, and aligned it so that the solar cell is uniformly irradiated. (See fig (4.7)).

Fig (4.4) Setup of experimental

4.5 Carrying out of the experiment:

- The circuit was closed, first shorting the variable resistor with an additional bridging plug, and choose the distance of the halogen lamp so that the short circuit current was determined.

- The shorting bridging plug was removed, and increases the terminal voltage or decrease the current, respectively, step by step by changing the load resistance. For each step the current and the voltage were read, and take them down.
- Then interrupt the circuit, and measured the open-circuit voltage.
- Repeat the series of measurements by change load resistance.

4.6Results

This section concerned with results and discussion. The results is concerned with samples characterization by Ultra violet-visible spectroscopy. Electrical circuit was used the I-V character is were studied by using (voltmeter, Ammeter and a light source Lamp).The solar cell was exposed to light and the current and voltages of the cell were recorded then one use the I-V characteristics were used to study performance .

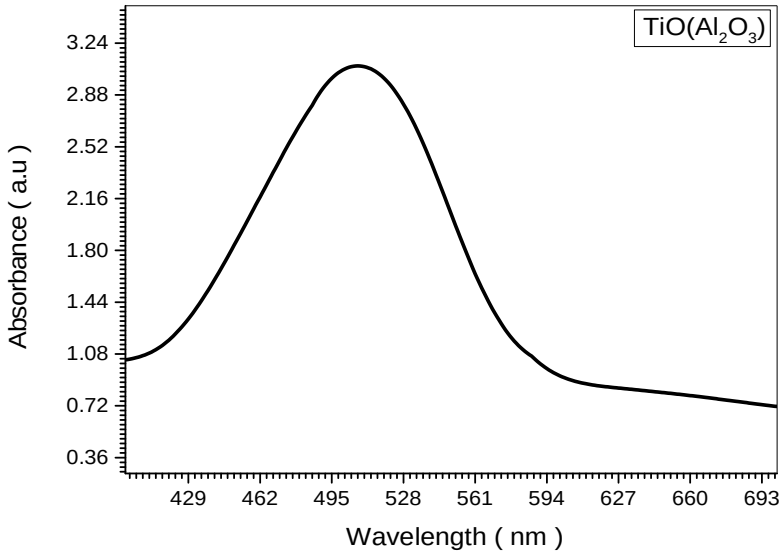

Fig (4.5)the UV Vis spectra optical absorbance of Ti Al_2 O_4 in room temperature

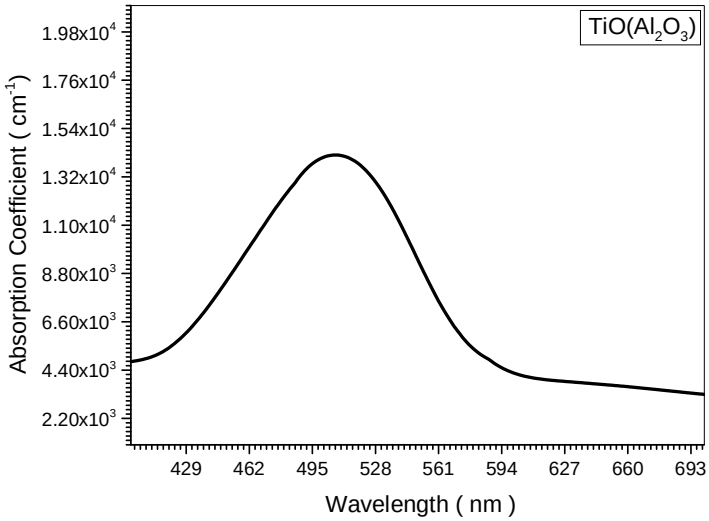

Fig (4.6)the spectra Absorption Coefficient Veers wavelength of Ti Al_2 O_4 in room temperature

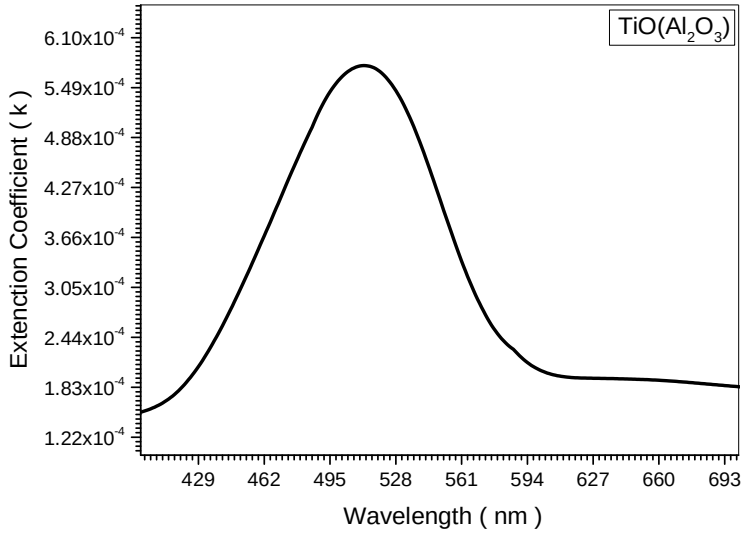

Fig (4.7)the spectra Extinction Coefficient Veers wavelength of Ti Al_2O_4 in room temperature

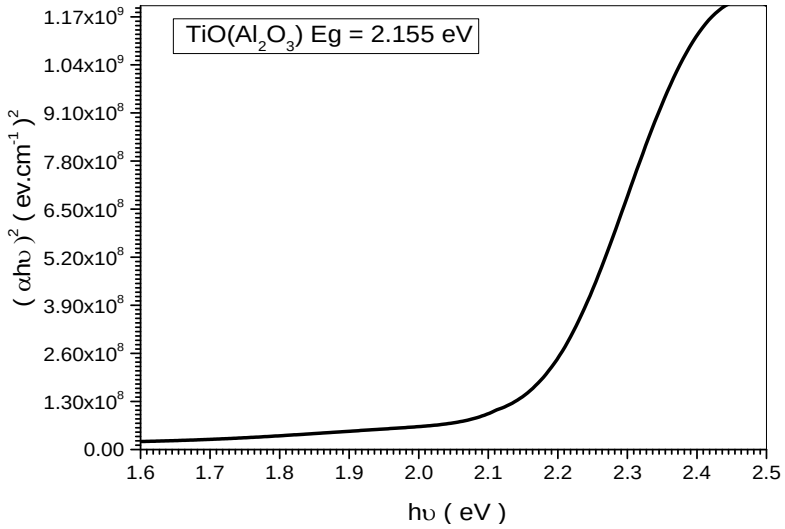

Fig (4.8)optical band gap energy (Eg) of Ti Al_2O_4 in room temperature

Table (4.1) I-V reaction for sample $TiAl_2O_3$

Voltage (V)	Current (mA)
0	53
0.02	53
0.03	53
0.04	53
0.05	53
0.17	53
0.2	53
0.3	52
0.4	48
0.45	36
0.48	0

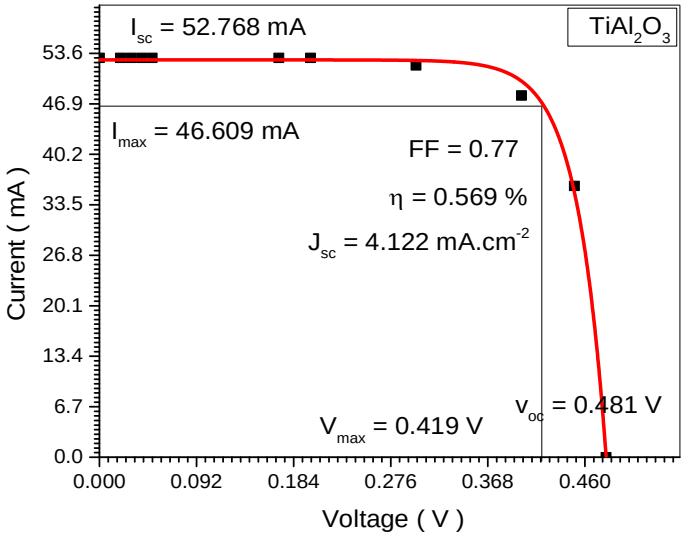

Fig (4.9)several factors for characterization of samples $TiAl_2O_3$

Discussion For Ti Al_2 O_4 sample :

The optical absorption spectrais in the (400 - 700) nm wavelength range as show in Fig (4.8). The maximum absorption is observed at wavelength

(510 nm). The absorption edge of the Ti Al_2 O_4 occurs at wavelength (510 nm) corresponding to photon energy (2.43 eV). Fig (4.9) shows the relation between absorption coefficient and wavelengths.Fig (4.2) show that the maximal value of absorption coefficient >1.32x10^4 cm^{-1} at (510 nm) for Ti Al_2 O_4 sample, and found rapid decrease after 510 nm wavelength.

The energy band gap of Ti Al_2 O_4 is determined using the absorption spectra. The value of the energy gap has been to found be (2.155 eV) as show in fig (4.11). Fig (4.12) shows the current-voltage characteristics the short-circuit current (I_{sc}) is 52.768 mA, the open-circuit voltage (V_{oc}) is 0.481 V, fill factor (FF) is 0.77, and the efficiency is 0.569 %.

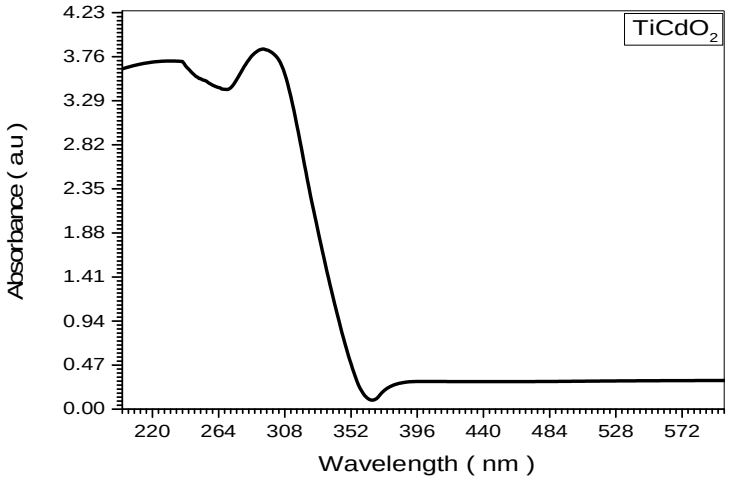

Fig (4.10) the UV Vis spectra optical absorbance of Ti Cd O_2 in room temperature

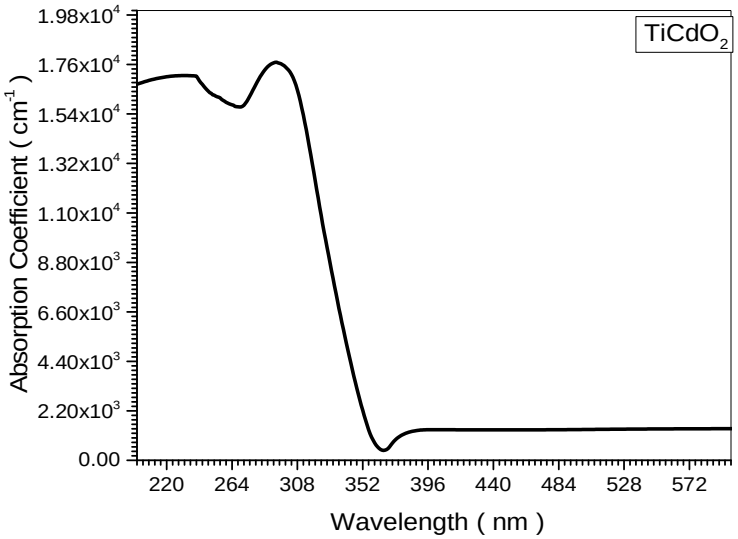

Fig (4.11)the spectra Absorption Coefficient Veers wavelength of Ti Cd O_2 in room temperature

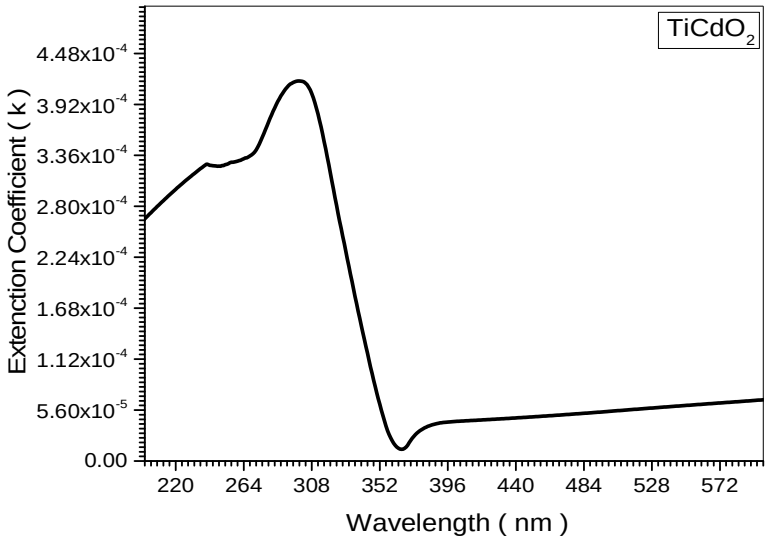

Fig (4.12)the spectra Extinction Coefficient Veers wavelength of Ti Cd O_2 in room temperature

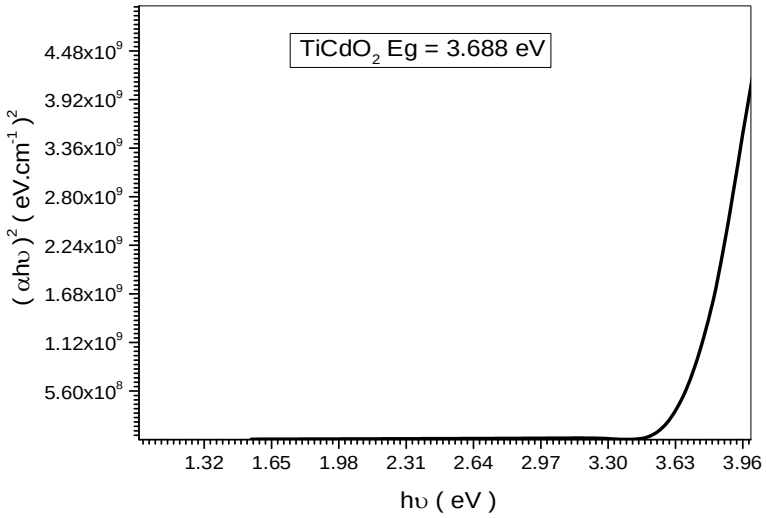

Fig (4.13)optical band gap energy (Eg) of Ti Cd O_2 in room temperature

Table (4.2) I-V reaction for sample Ti Cd O_2

Voltage (V)	Current (mA)
0	50
0.03	50
0.04	50
0.1	50
0.11	50
0.15	43
0.16	31
0.18	0

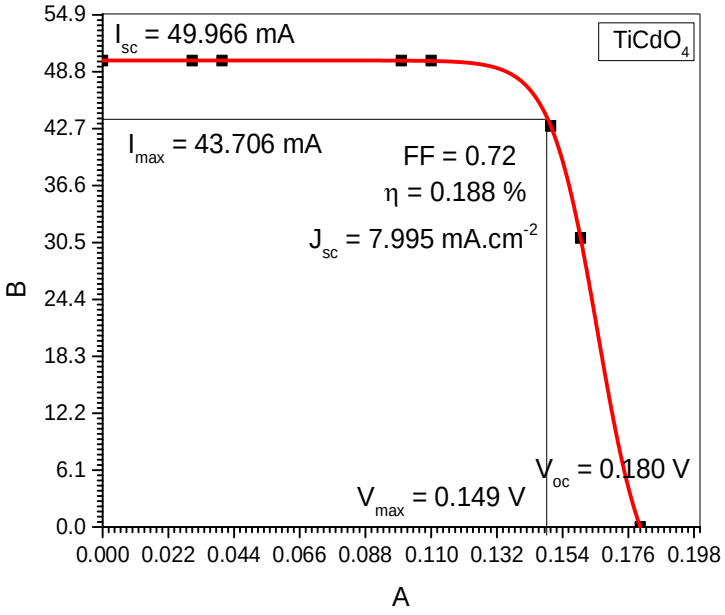

Fig(4.14)several factors for characterization of samples Ti CdO_2

Discussion for Ti CdO_2 sample :

The absorption spectra in the (200 - 600) nm wavelength range as show in Fig (4.13). The maximum absorption is observed at wavelength (308 nm). of the Ti Cd O_2 occurs at wavelength (510 nm) corresponding to photon energy (4.026 eV). Fig (4.14) shows the relation between absorption coefficient and wavelengths. Also in fig (4.14) show that the maximal value of absorption coefficient $>1.7x10^4$ cm^{-1} at (308 nm) and found rapid decrease after 308 nm wavelength. The value of the energy gap has been to found be (3.688 eV) as show in fig (4.16). Fig (4.17) shows the current-voltage characteristics obtained from the measured values. This measurement was taken from solar cell of Ti Cd O_2 the short-circuit current (I_{sc}) is 49.966 mA, the open-circuit voltage (V_{oc}) is 0.180 V, fill factor (FF) is 0.72, and the efficiency is 0.188 %.

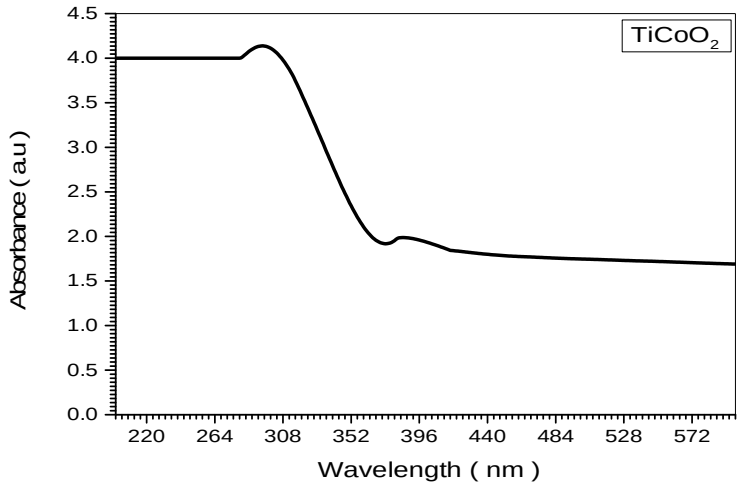

Fig (4.15)the UV Vis spectra optical absorbance of Ti Co O_2 in room temperature

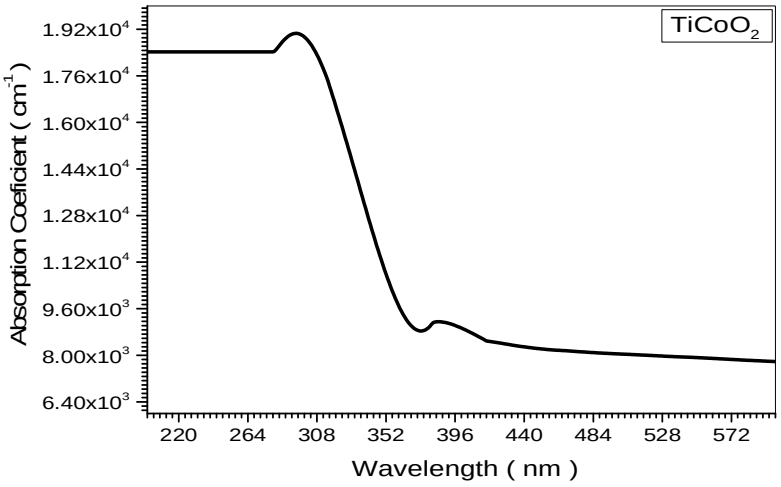

Fig (4.16)the spectra Absorption Coefficient Veers wavelength of Ti Co O_2 in room temperature

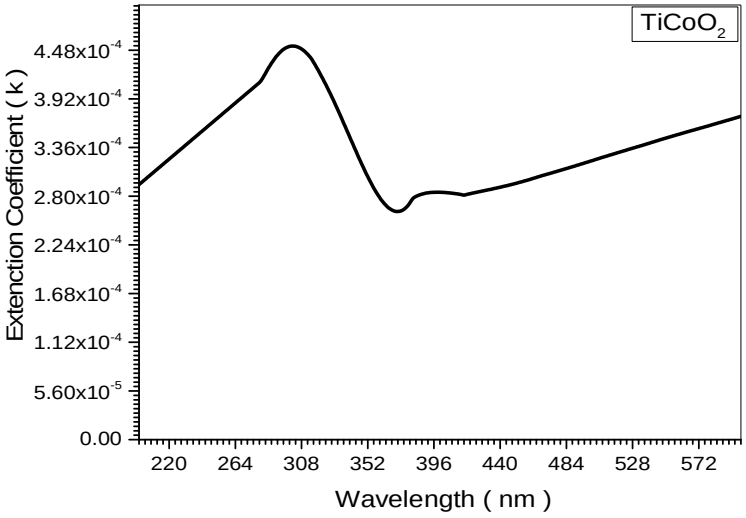

Fig (4.17)the spectra Extinction Coefficient Veers wavelength of Ti Co O_2 in room temperature

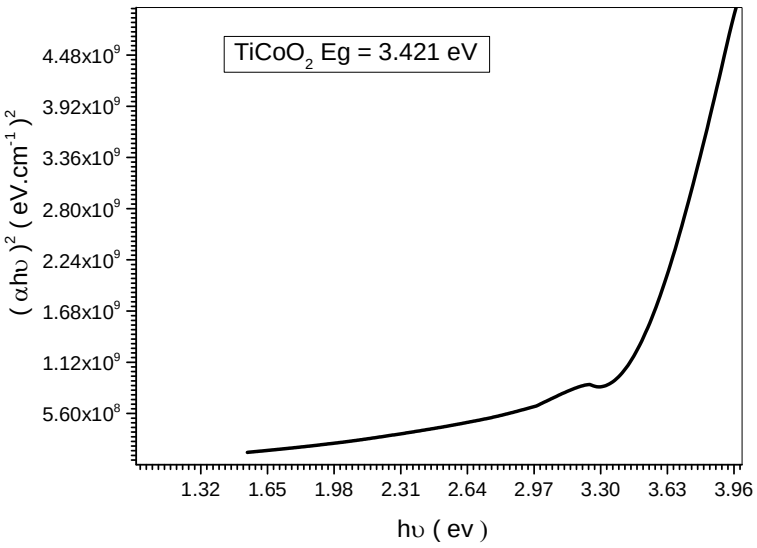

Fig (4.18)optical band gap energy (Eg) of Ti Co O_2 in room temperature

Table (4.3) I-V reaction for sample Ti Co O_2

Voltage (V)	Current (mA)
0	40
0.01	40
0.02	40
0.06	40
0.11	40
0.12	40
0.18	40
0.23	36
0.26	0

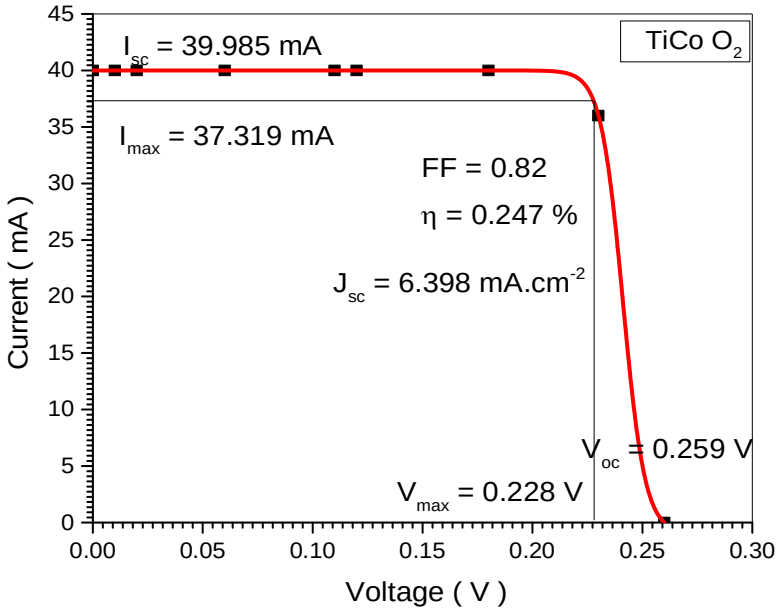

Fig (4.19)several factors for characterization of samples $TiCoO_2$

Discussion for$TiCoO_2$ sample :

The optical absorption spectra in the (200 - 600) nm wavelength as show in Fig (4.18). The maximum absorption is observed at wavelength (308 nm) occurs at wavelength (308 nm) corresponding to photon energy

(4.026 eV). Fig (4.19) shows the relation between absorption coefficient and wavelengths .Also in fig (4.19) show that the maximal value of absorption coefficient $>1.7x10^4$ cm^{-1} at (308 nm) . The value of the energy gap has been to found be (3.421 eV) as show in fig (4.22). Fig (4.23) shows the current-voltage characteristics obtained from the measured values. This measurement was taken from solar cell of the short-circuit current (I_{sc}) is 39.985 mA, the open-circuit voltage (V_{oc}) is 0.259 V, fill factor (FF) is 0.82, and the efficiency is 0.247 %.

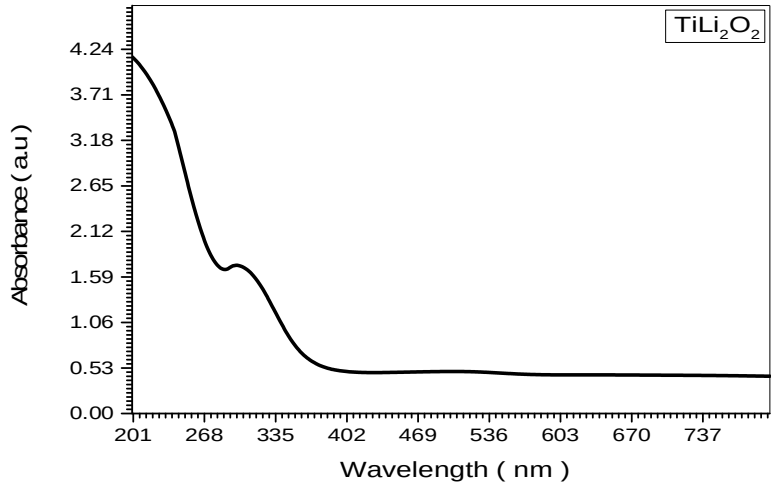

Fig (4.20)the UV Vis spectra optical absorbance of Ti Li_2 O_2 in room temperature

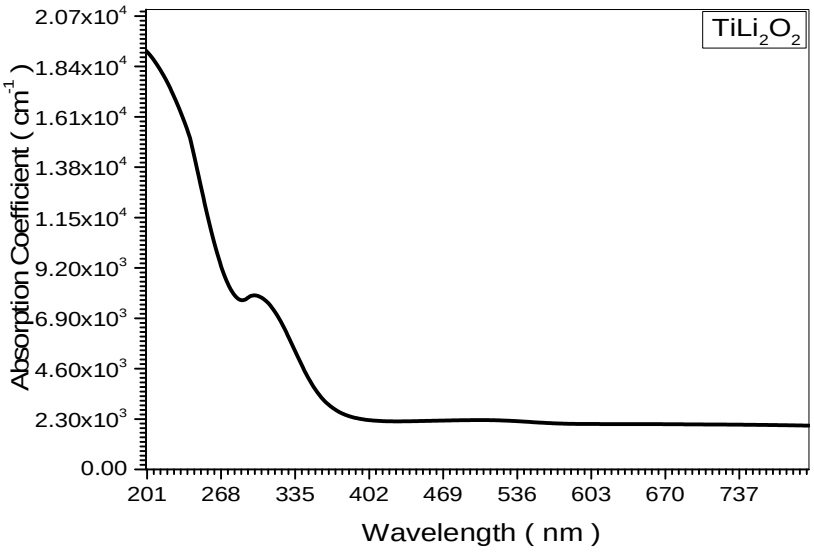

Fig (4.21)the spectra Absorption Coefficient Veers wavelength of Ti Li_2 O_2 in room temperature

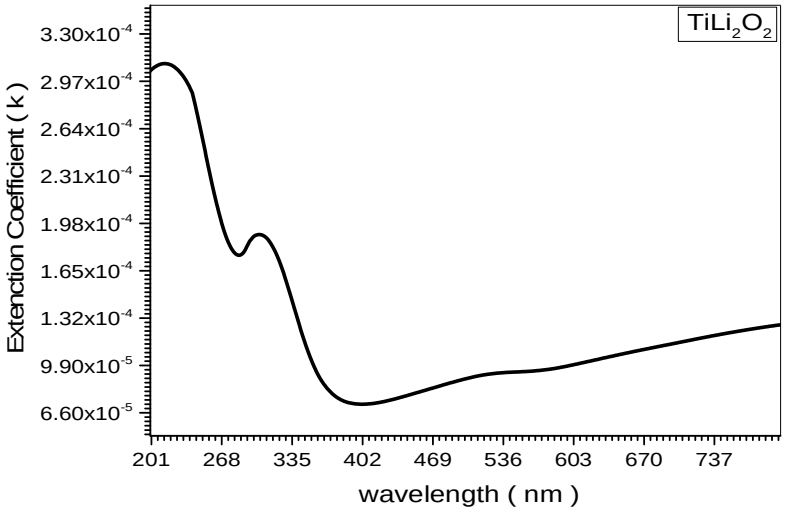

Fig (4.22)the spectra Extinction Coefficient Veers wavelength of Ti Li_2 O_2 in room temperature

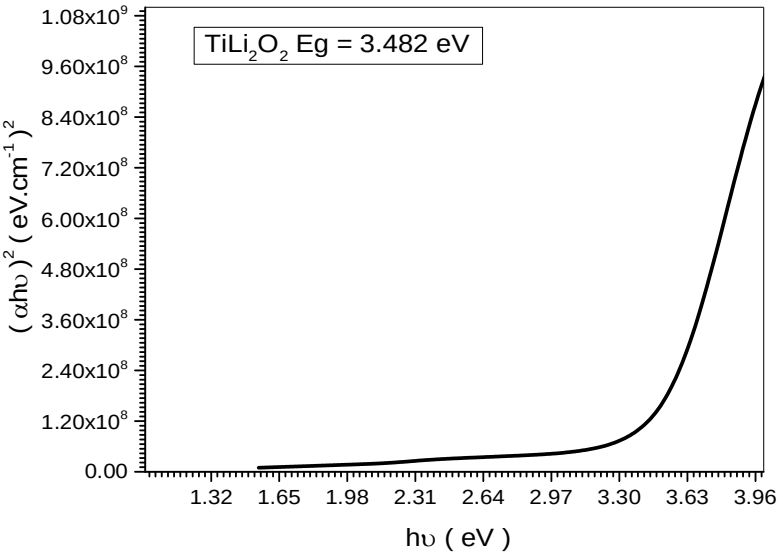

Fig (4.23)optical band gap energy (Eg) of Ti Li_2O_2 in room temperature

Table (4.4) I-V reaction for sample Ti Li_2O_2

Voltage (V)	Current (mA)
0	48
0.02	48
0.03	48
0.04	48
0.05	48
0.21	48
0.31	47
0.41	32
0.45	0

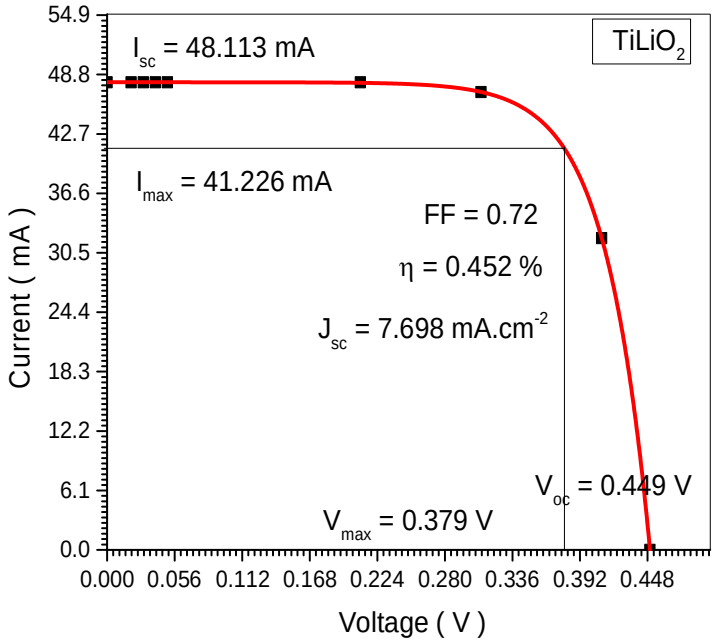

Fig (4.24)several factors for characterization of samples $TiLi_2O_2$

Discussion for$TiLi_2O_2$sample:

The optical absorption spectra in the (200 - 700) nm wavelength range as shown inFig (4.24). The maximum absorption is observed at wavelength (201 nm) at wavelength (510 nm) corresponding to photon energy (6.17 eV). Fig (4.25) shows the relation between absorption coefficient and wavelengths .Also in fig (4.25) show that the maximal value of absorption coefficient $>1.84x10^4$ cm^{-1} at (201 nm).The value of the energy gap of $TiLi_2O_2$ is determined using the absorption spectra .the value of the energy gap has been to fond be (3.482 eV) as shown in fig (4.27). Fig (4.28) shows the current-voltage characteristics where the short-circuit current (I_{sc}) is 48.113 mA, the open-circuit voltage (V_{oc}) is 0.449 V, fill factor (FF) is 0.72, and the efficiency is 0.452 %.

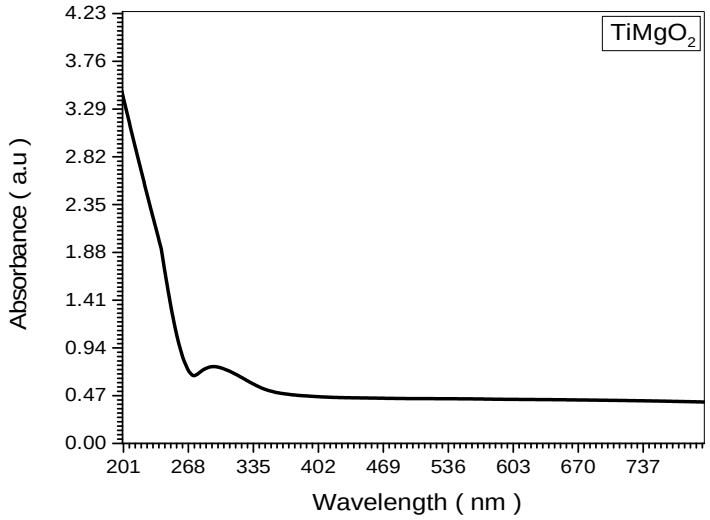

Fig (4.25) the UV Vis spectra optical absorbance of Ti Mg O_2 in room temperature

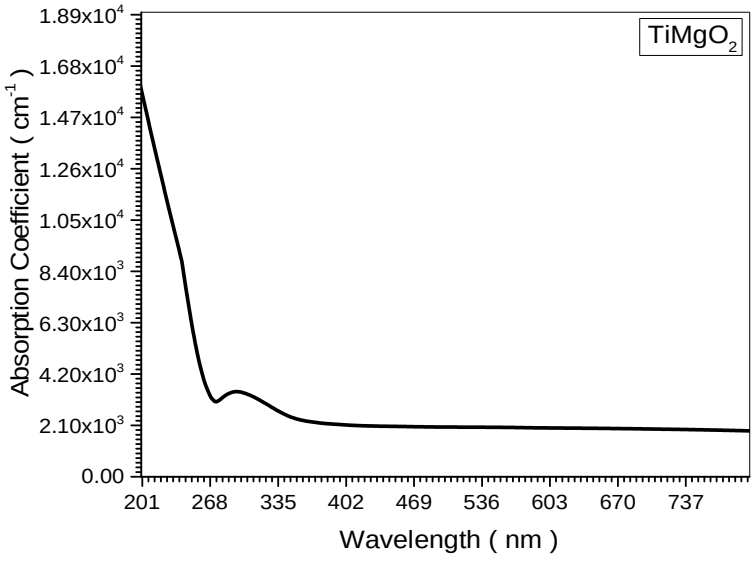

Fig (4.26) the spectra Absorption Coefficient Veers wavelength of Ti Mg O_2 in room temperature

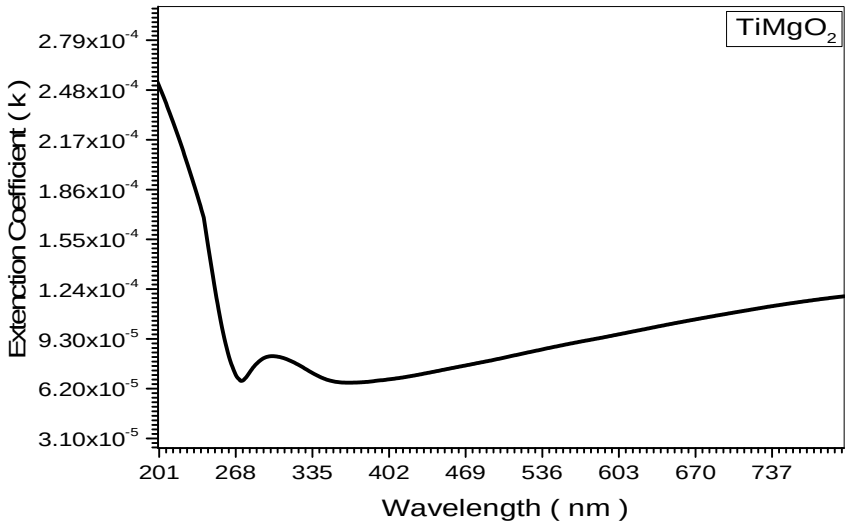

Fig (4.27) the spectra Extinction Coefficient Veers wavelength of Ti Mg O_2 in room temperature

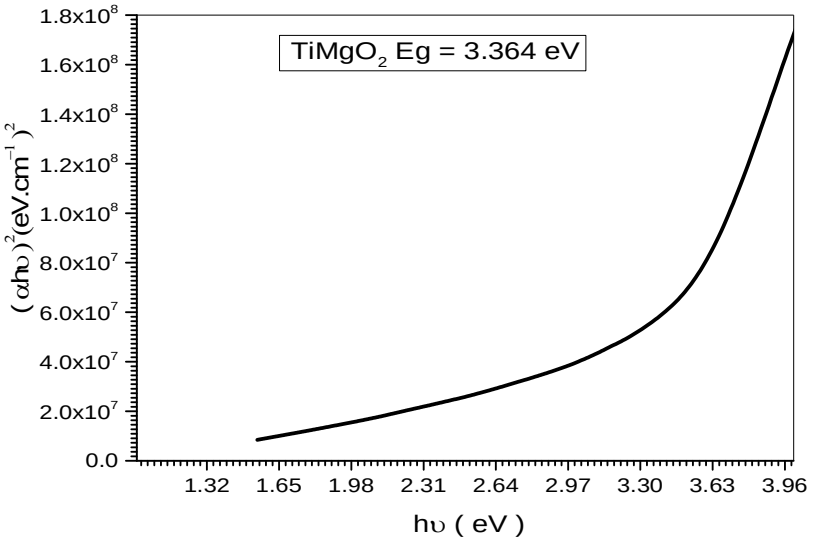

Fig (4.28) optical band gap energy (Eg) of Ti Mg O_2 in room temperature

Table (4.5) I-V reaction for sample Ti Mg O_2

Voltage (V)	Current (mA)
0	33
0.02	33
0.04	33
0.05	33
0.1	33
0.2	33
0.4	32
0.6	24
0.65	0

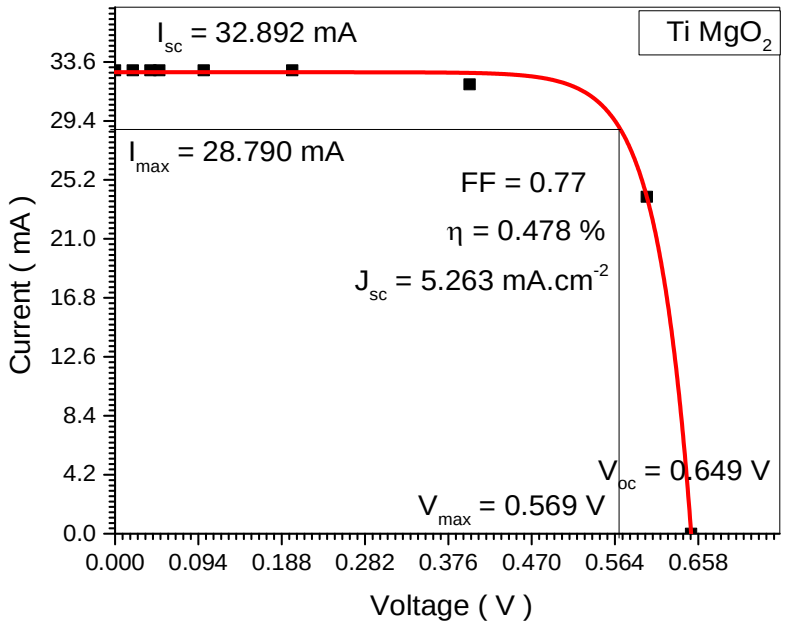

Fig (4.29)several factors for characterization of samples Ti Mg O_2

Discussion forTi Mg O_2 sample:

The optical absorption spectra is in the (400 - 700) nm wavelength range as shown inFig (4.29). The maximum absorption is observed at wavelength (201 nm). at wavelength (201 nm) corresponding to photon

energy (6.17 eV). Fig (4.30) shows the relation between absorption coefficient and wavelengths .Also in fig (4.30) shows that the maximal value of absorption coefficient >1.47x10^4 cm^{-1} at (201 nm) for Ti Mg O_2 sample and found rapid decrease after 201 nm wavelength. The value of the energy gap of Ti Mg O_2 determined tousing absorption spectra. The value of the energy gap has been to found be (3.364 eV) as shown in fig (4.32). Fig (4.33) shows the current-voltage characteristics where short-circuit current (I_{sc}) is 32.89 mA, the open-circuit voltage (V_{oc}) is 0.649 V, fill factor (FF) is 0.82, and the efficiency is 0.478 %.

Table (4.6) is Factors for characterization of Ti doping by different Oxides solar cells performance for five samples

Sample	η %	E_g (eV)	J_{sc} ($mA.cm^{-2}$)	FF
$TiAl_2O_3$	0.569	2.155	4.122	0.77
$TiCdO_4$	0.188	3.688	7.995	0.72
$TiCoO_2$	0.247	3.421	6.398	0.82
Ti Li_2 O_2	0.452	3.482	7.698	0.72
$TiMgO_2$	0.478	3.364	5.263	0.77

Table (4.7) is Factors for characterization of Ti doping by different Oxides solar cells performance for five samples

Sample	I_{sc} (mA)	I_{max}(mA)	V_{oc}(V)	V_{max}(V)
$TiAl_2O_3$	52.768	46.609	0.481	0.419
$TiCdO_4$	49.966	43.706	0.180	0.149
$TiCoO_2$	39.985	37.319	0.259	0.228
Ti Li_2 O_2	48.113	41.226	0.449	0.379
$TiMgO_2$	32.892	28.790	0.649	0.569

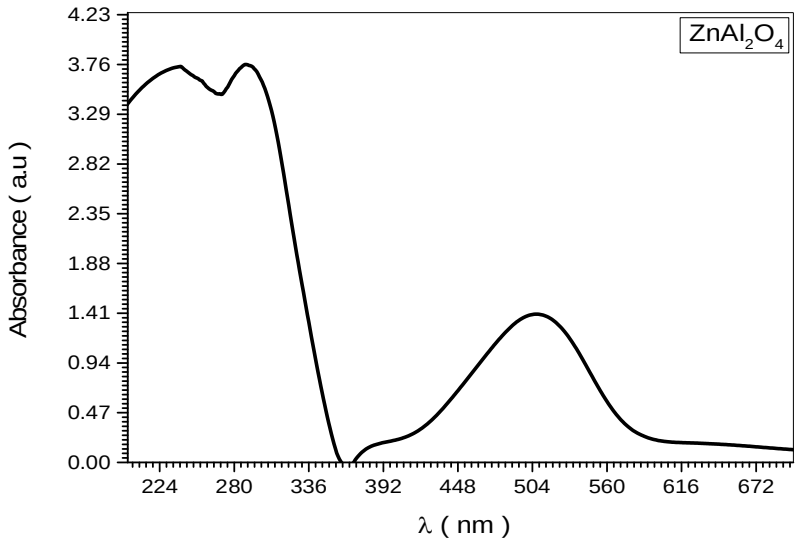

Fig (4.29)the spectra Absorption Coefficient Veers wavelength of Zn Al_2 O_4 in room temperature

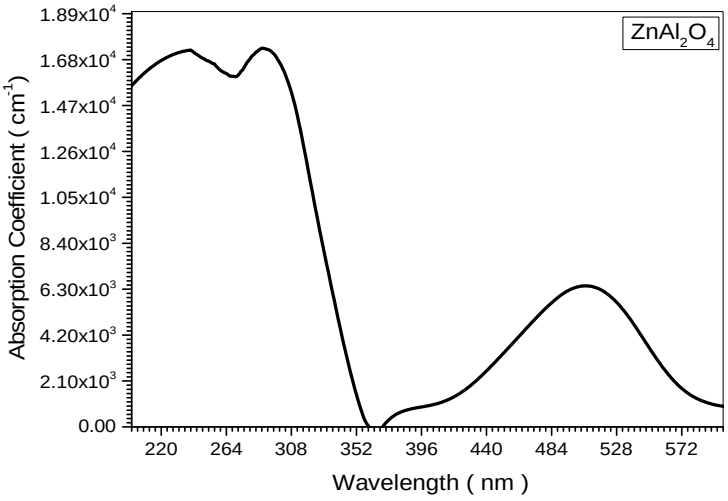

Fig (4.30)the spectra Absorption Coefficient Veers wavelength of Zn Al_2 O_4 in room temperature

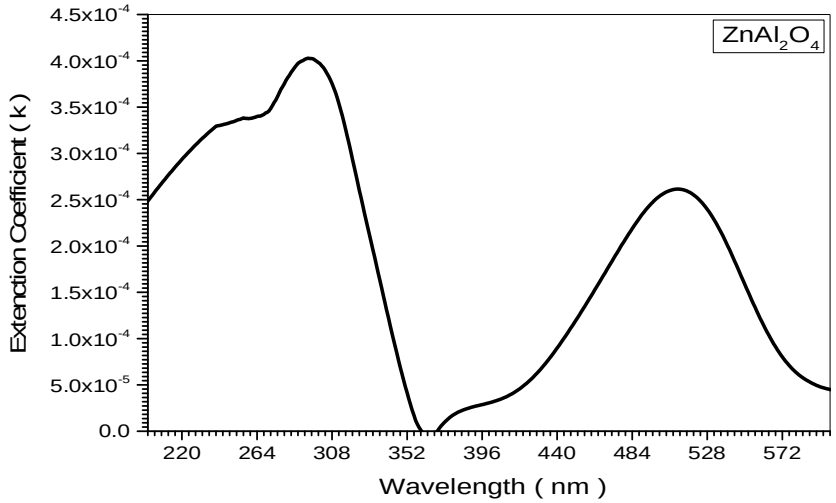

Fig (4.31)the spectra Extinction Coefficient Veers wavelength of Zn Al_2 O_4 in room temperature

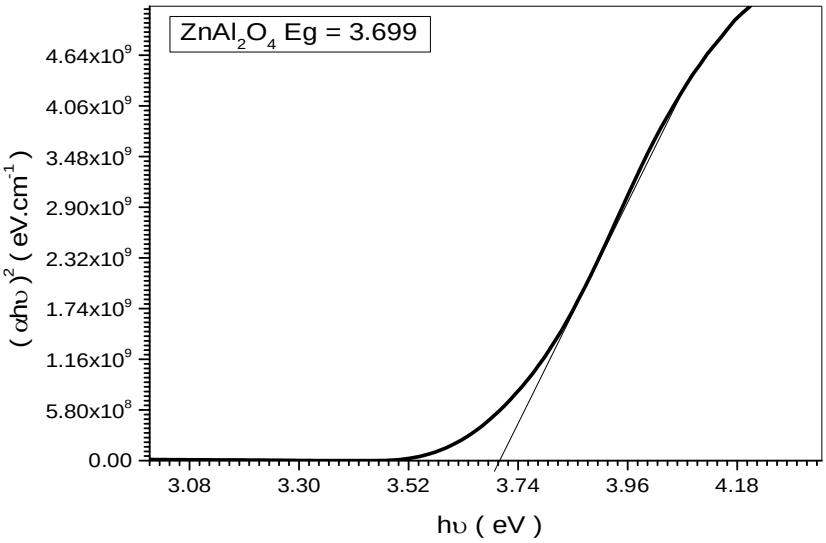

Fig (4.32)optical band gap energy (Eg) of Zn Al_2 O_4 in room temperature

Table (4.8) I-V reaction for sample Zn Al_2 O_4

Voltage (V)	Current (mA)
0	47
0.03	47
0.04	47
0.06	47
0.1	47
0.12	46
0.13	41
0.14	36
0.145	0

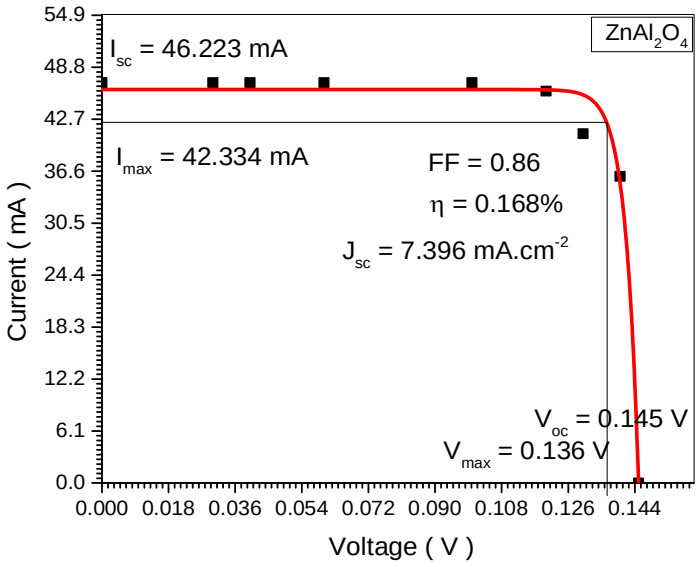

Fig (4.33)several factors for characterization of samples Zn Al_2 O_4

for Zn Al_2 O_4 sample :

The optical absorption spectra is in the (200 - 800) nm wavelength of Zn Al_2O_4 as shown in Fig (4.34). The maximum absorption is observed at wavelength (320 nm) at wavelength (320 nm) corresponding to photon energy (3.875 eV). Fig (4.35) shows the relation between absorption coefficient and wavelengths .Also in fig (4.35) shows that the maximal value of absorption coefficient >$1.68x10^4$ cm^{-1} at (320 nm) and for Zn Al_2 O_4 samples. The value of the energy gap of Zn Al_2 O_4 determined using the absorption spectra. The value of the energy gap has been to found be (3.699 eV) as shown in fig (4.37).Fig (4.38) shows the current-voltage characteristics where the short-circuit current (I_{sc}) is 46.223 mA, the open-circuit voltage (V_{oc}) is 0.145 V, fill factor (FF) is 0.86, and the efficiency is 0.168 %.

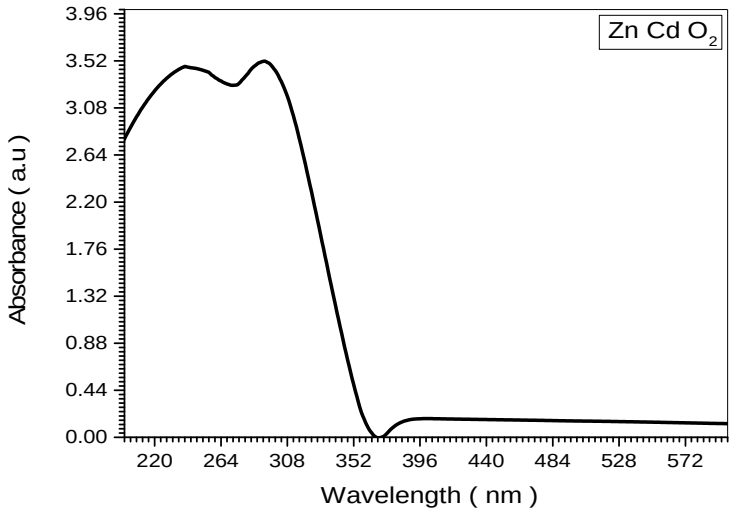

Fig (4.34) the spectra Absorption Coefficient Veers wavelength of Zn Cd O_2 in room temperature

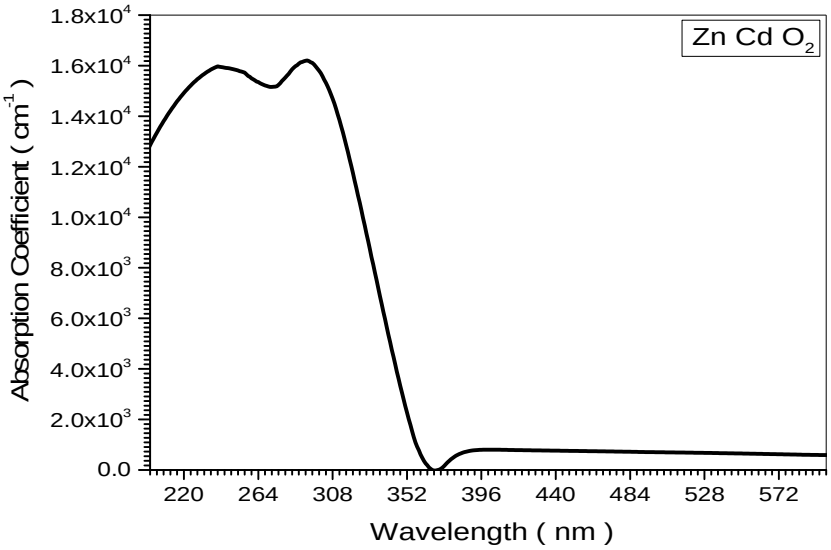

Fig (4.35)the spectra Absorption Coefficient Veers wavelength of Zn Cd O_2 in room temperature

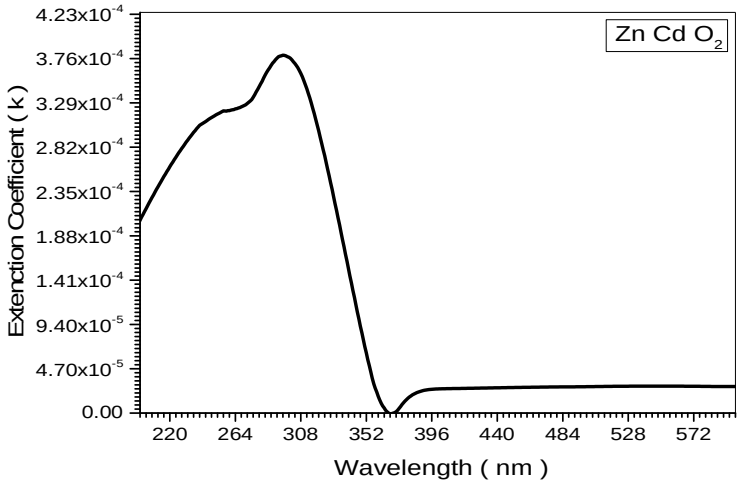

Fig (4.36)the spectra Extinction Coefficient Veers wavelength of Zn Cd O_2 in room temperature

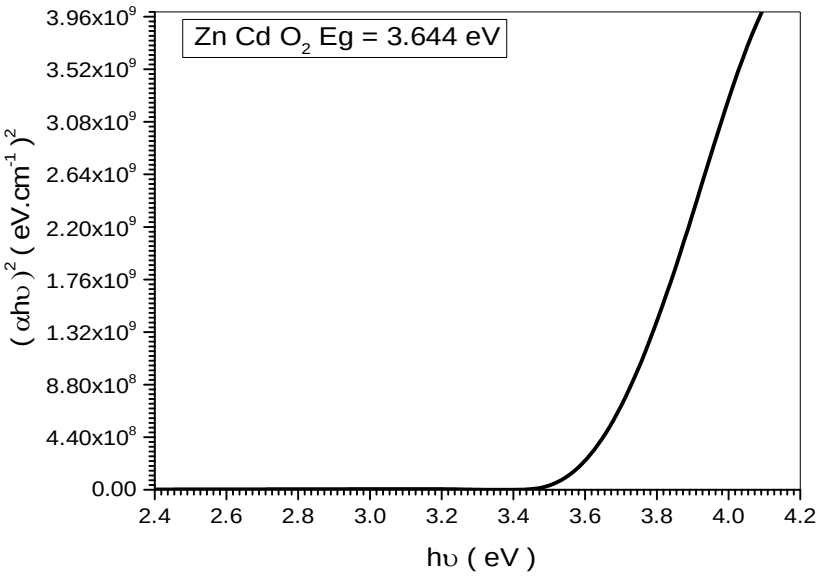

Fig (4.37)optical band gap energy (Eg) of Zn Cd O_2 in room temperature

Table (4.9) I-V reaction for sample Zn Cd O_2

Voltage (V)	Current (mA)
0.000	46
0.037	46
0.049	46
0.074	46
0.123	46
0.147	46
0.159	41
0.172	36
0.178	0

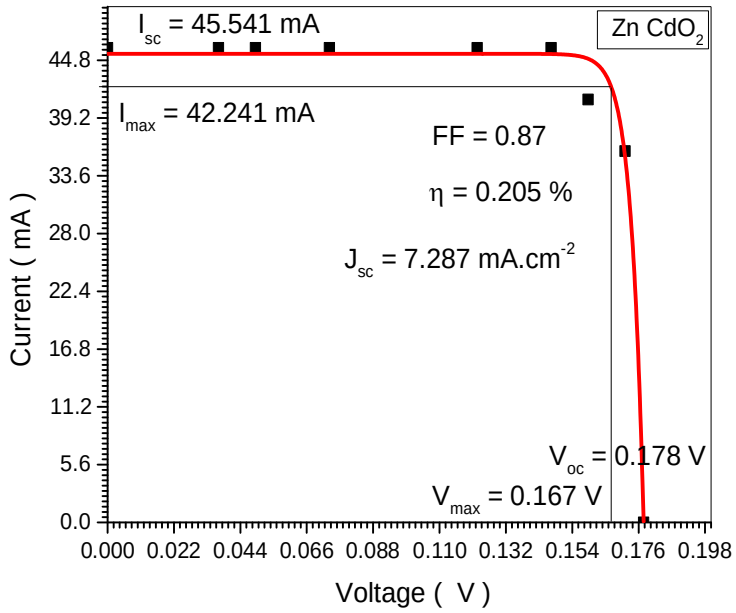

Fig (4.38)several factors for characterization of samples Zn Cd O_2

forZn Cd O_2:

The optical absorption spectrais in the (200 - 600) nm wavelength range for the Zn Cd O_2 was depicted in Fig (4.39). The maximum absorption is observed at wavelength (310 nm). The absorption edge of the Zn Cd O_2 occurs at wavelength (310 nm) corresponding to photon energy (4 eV). In fig (4.40) show that the maximal value of absorption coefficient $>1.6x10^4$ cm^{-1} at (310 nm) for Zn Cd O_2 sample .The energy band gap found be (3.644 eV) as shown in fig (4.42). In Fig (4.43) shows the current-voltage characteristics where the short-circuit current (I_{sc}) is 45.541 mA, the open-circuit voltage (V_{oc}) is 0.178 V, fill factor (FF) is 0.87, and the efficiency is 0.205 %.

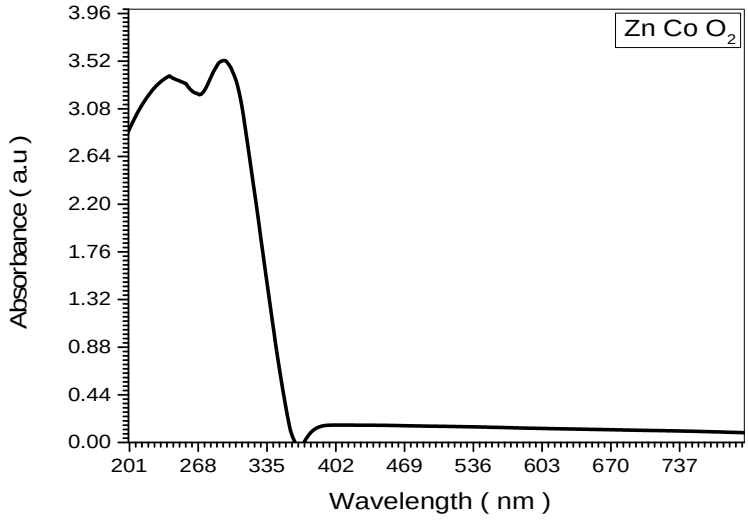

Fig (4.39)the spectra Absorption Coefficient Veers wavelength of Zn Co O_2 in room temperature

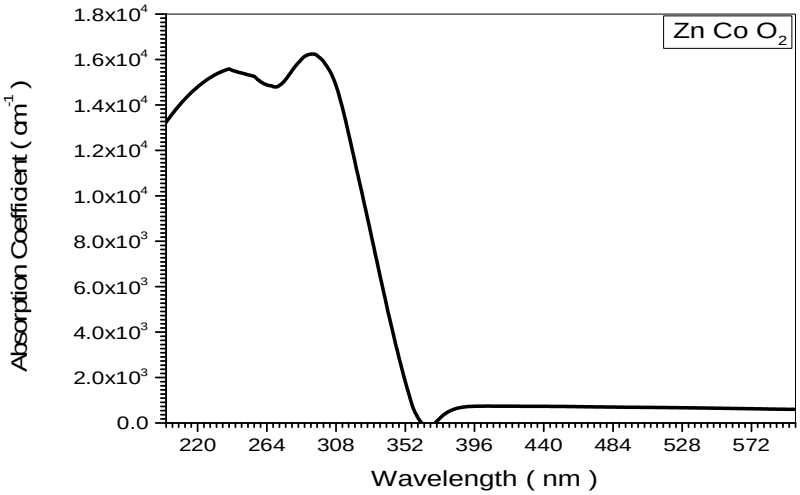

Fig (4.40)the spectra Absorption Coefficient Veers wavelength of Zn Co O_2 in room temperature

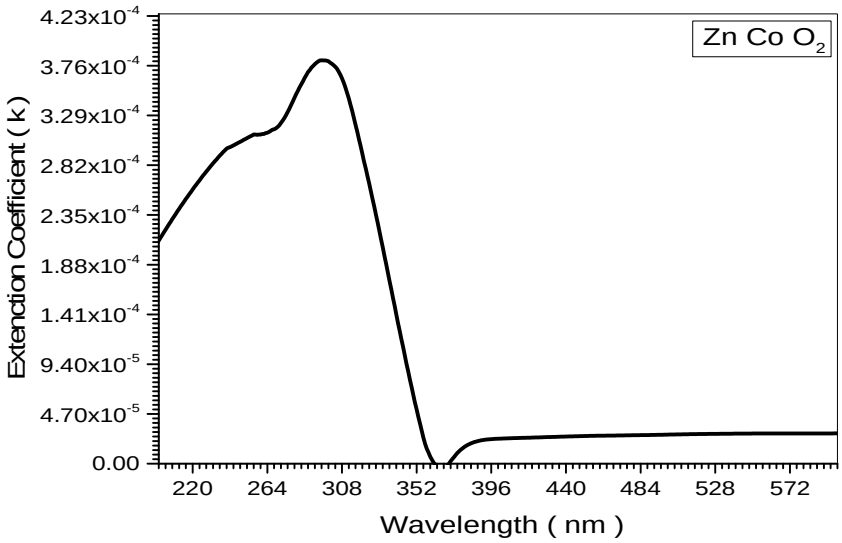

Fig (4.41)the spectra Extinction Coefficient Veers wavelength of Zn Co O_2 in room temperature

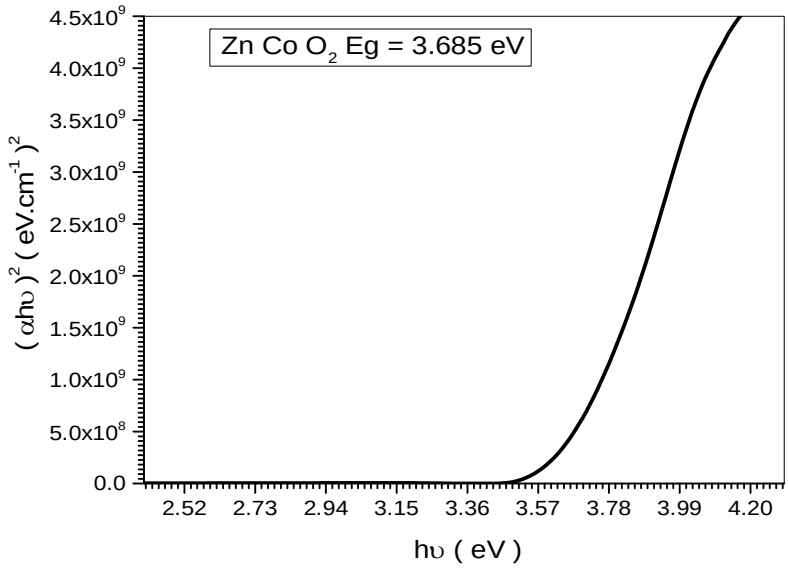

Fig (4.42)optical band gap energy (Eg) of Zn Co O_2 in room temperature

Table (4.10) I-V reaction for sample Zn Co O_2

Voltage (V)	Current (mA)
0	43
0.04	43
0.05	43
0.08	43
0.13	43
0.16	43
0.17	41
0.19	36
0.20	0

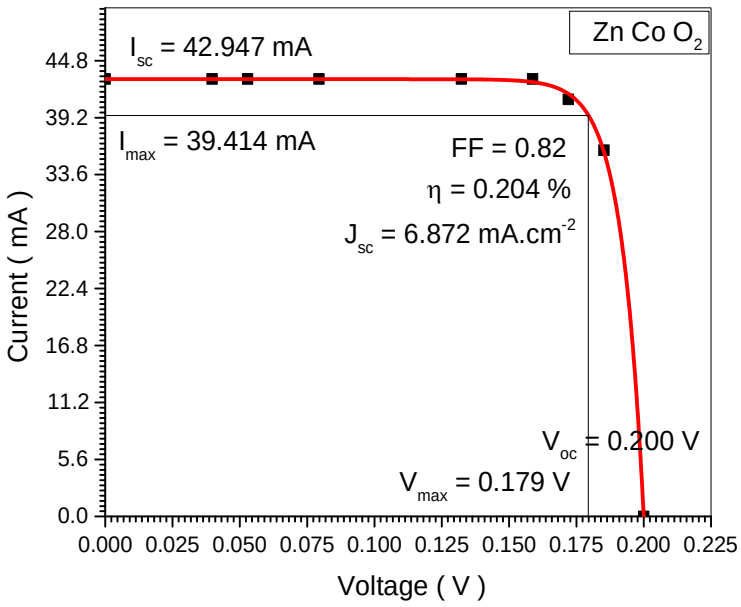

Fig (4.43)several factors for characterization of samples Zn Co O_2

forZn Co O_2 :

The optical absorption spectra is in the (200 - 750) nm wavelength range for the Zn Co O_2 was depicted in Fig (4.44). The maximum absorption is observed at wavelength (325 nm). The absorption edge of the Zn Co O_2 occurs at wavelength (325 nm) corresponding to photon energy (3.82 eV). In fig (4.45) show that the maximal value of absorption coefficient $>1.6x10^4$ cm^{-1} at (325 nm) for Zn Co O_2 sample. The energy band gap of Zn Co O_2 is determined using the absorption spectra has been to found be (3.685 eV) as shown in fig (4.47). Fig (4.48) shows the current-voltage characteristics where the short-circuit current (I_{sc}) is 42.947 mA, the open-circuit voltage (V_{oc}) is 0.200 V, fill factor (FF) is 0.82, and the efficiency is 0.204 %.

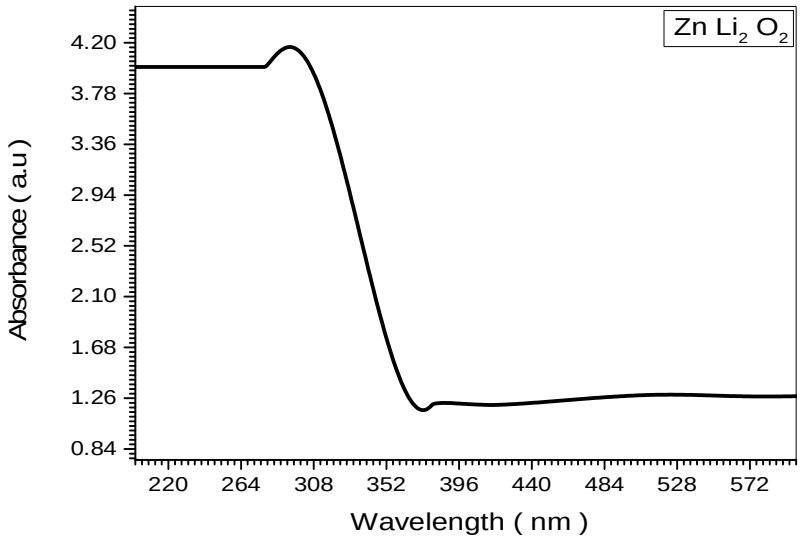

Fig (4.44)the spectra Absorption Coefficient Veers wavelength of Zn Li_2 O_2 in room temperature

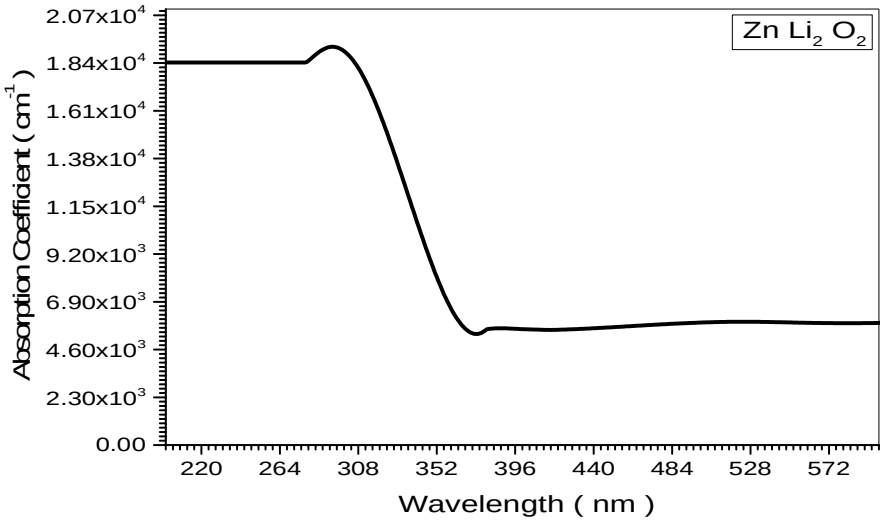

Fig (4.45)the spectra Absorption Coefficient Veers wavelength of Zn Li_2 O_2 in room temperature

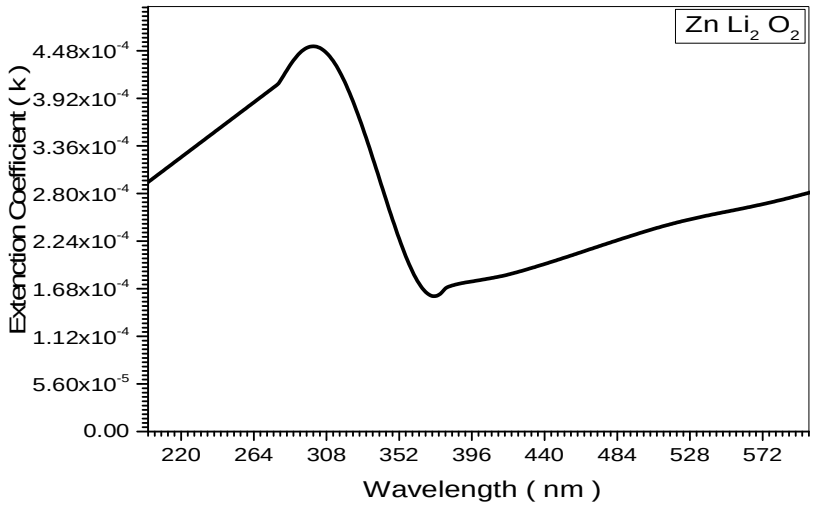

Fig (4.46)the spectra Extinction Coefficient Veers wavelength of Zn Li_2 O_2 in room temperature

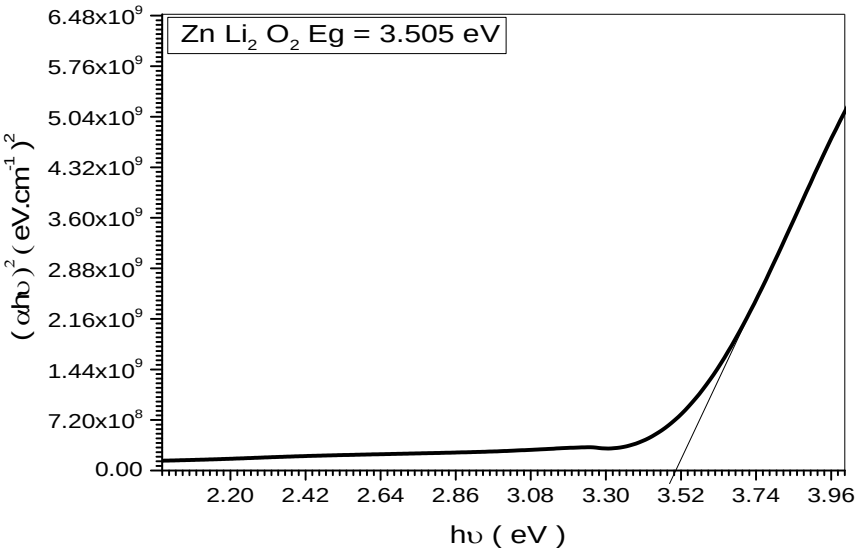

Fig (4.47)optical band gap energy (Eg) of Zn Li_2 O_2 in room temperature

Table (4.11) I-V reaction for sample Zn Li_2 O_2

Voltage (V)	Current (mA)
0.000	46
0.054	46
0.072	46
0.108	46
0.179	46
0.215	46
0.233	41
0.251	36
0.260	0

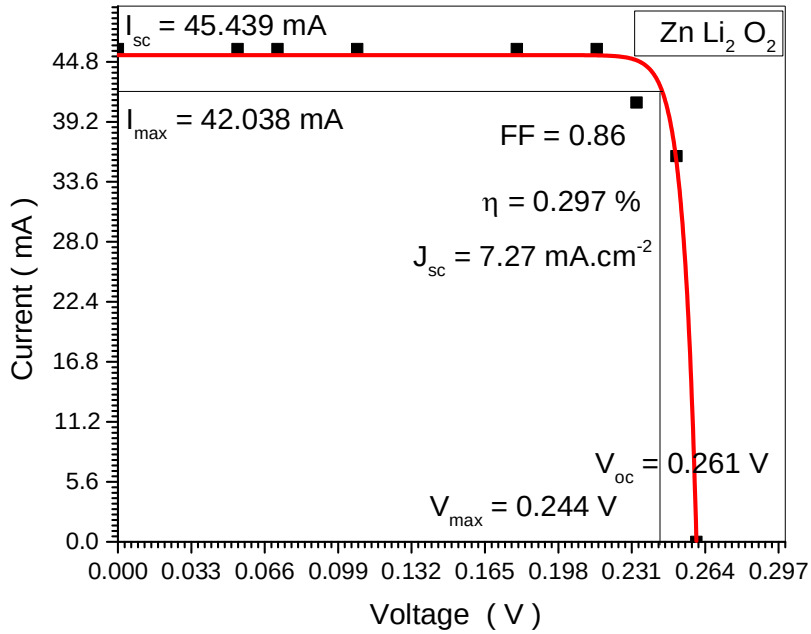

Fig (4.48)several factors for characterization of samples Zn Li_2 O_2

forZn Li_2 O_2:

The optical absorption spectra is in the (200 - 600) nm wavelength as shown in Fig (4.49). The maximum absorption is observed at wavelength (308 nm). The absorption edge of the Zn Li_2 O_2 occurs at wavelength (308 nm) corresponding to photon energy (4.026 eV) .In fig (4.50) shows that the maximal value of absorption coefficient >$1.84x10^4$ cm^{-1} at (308 nm) for Zn Li_2 O_2 sample, and found rapid decrease after 308 nm wavelength.The energy band gap of Zn Li_2 O_2 is determined using the absorption spectra wherethe value of the energy gap has been to found be (3.505 eV) as show in fig (4.52). Fig (4.53) shows the current-voltage characteristics where the short-circuit current (I_{sc}) is 45.439 mA, the open-circuit voltage (V_{oc}) is 0.261 V, fill factor (FF) is 0.86, and the efficiency is 0.297 %.

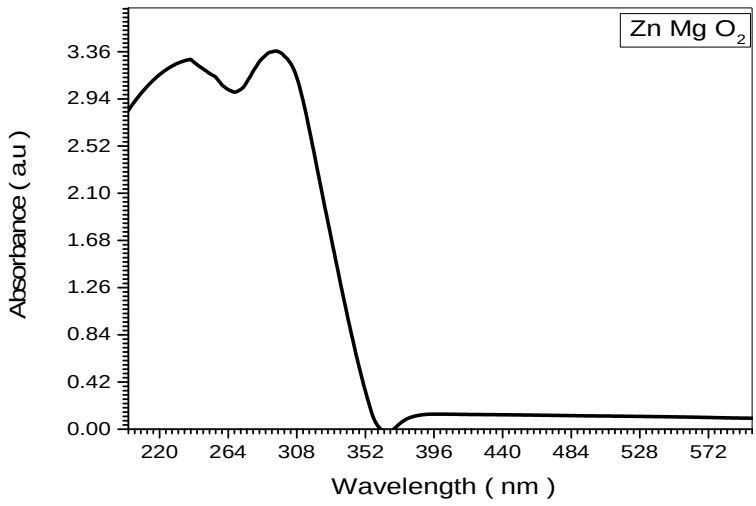

Fig (4.49)the spectra Absorption Coefficient Veers wavelength of Zn Mg O_4 in room temperature

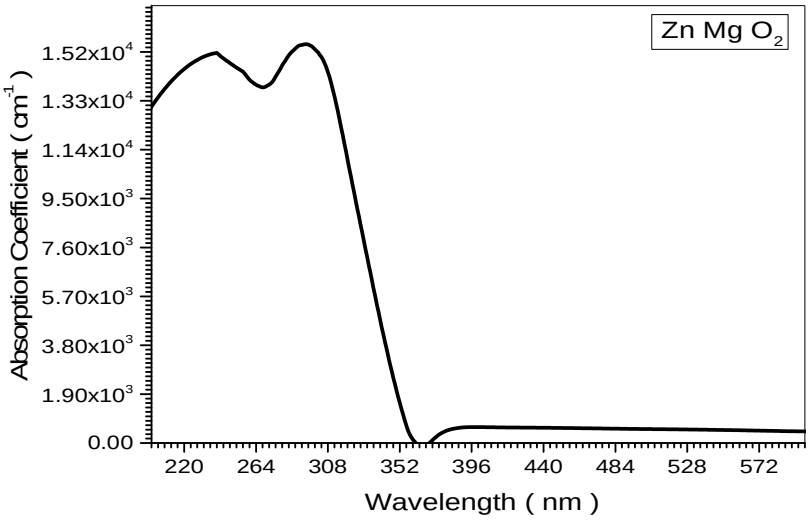

Fig (4.50) the spectra Absorption Coefficient Veers wavelength of Zn Mg O_2 in room temperature

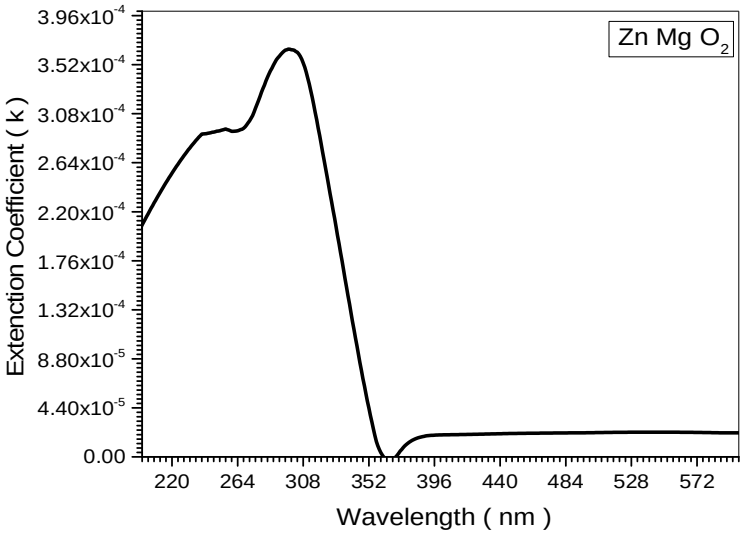

Fig (4.51)the spectra Extinction Coefficient Veers wavelength of Zn Mg O_2 in room temperature

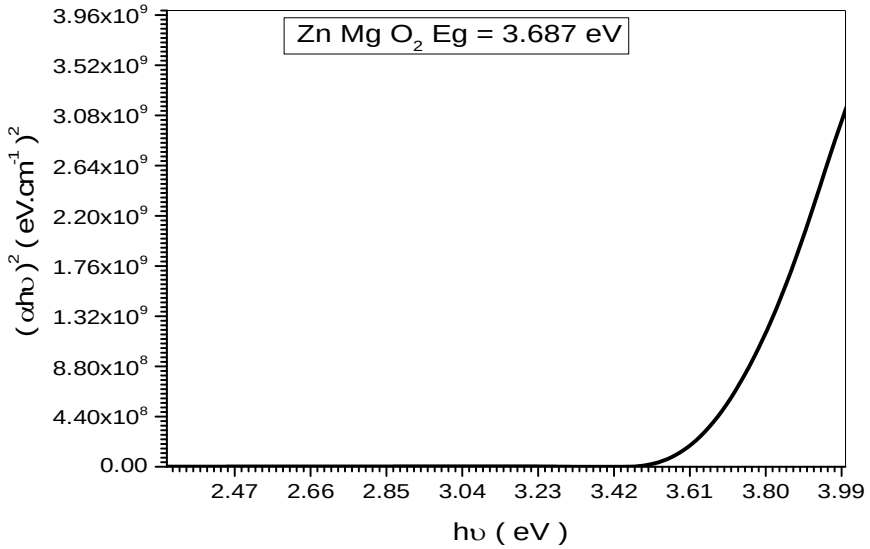

Fig (4.52)optical band gap energy (Eg) of Zn Mg O_2 in room temperature

Table (4.12) I-V reaction for sample Zn Mg O_2

Voltage (V)	Current (mA)
0.000	46
0.035	46
0.047	46
0.071	46
0.118	46
0.141	41
0.15	38
0.165	32
0.171	0

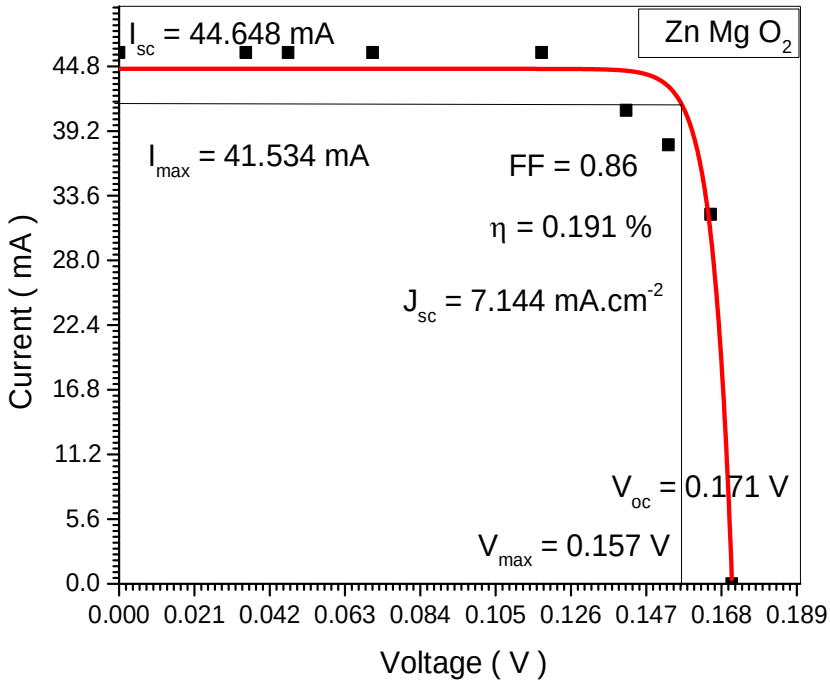

Fig (4.53)several factors for characterization of samples Zn Mg O_2

for Zn Mg O_2 :

The optical absorption spectrais in the (200 - 600) nm wavelength as shown in Fig (4.54). The maximum absorption is observed at wavelength (310 nm). The absorption edge of the Zn Mg O_2 occurs at wavelength (310 nm) corresponding to photon energy (4 eV). In fig (4.55) show that the maximal value of absorption coefficient $>1.4x10^4$ cm^{-1} at (310 nm) for Zn Mg O_2 sample, and found rapid decrease after 310 nm wavelength. The energy band gap of Zn Mg O_2 is determined using the absorption spectra. The value of the energy gap has been to found be (3.687 eV) as show in fig (4.57). Fig (4.58) shows the current-voltage characteristics where the short-circuit current (I_{sc}) is 44.698 mA, the open-circuit voltage (V_{oc}) is 0.171 V, fill factor (FF) is 0.86, and the efficiency is 0.191 %.

Table (4.13) is Factors for characterization of Zn doping by different Oxides solar cells performance for five samples

Sample	η %	E_g (eV)	J_{sc} ($mA.cm^{-2}$)	FF
$ZnAl_2O_3$	0.168	3.699	7.396	0.86
$ZnCdO_4$	0.205	3.644	7.287	0.87
$ZnCoO_2$	0.204	3.685	6.872	0.82
Zn Li_2 O_2	0.297	3.505	7.270	0.86
$ZnMgO_2$	0.191	3.687	7.144	0.86

Table (4.14) is Factors for characterization of Zn doping by different Oxides solar cells performance for five samples

Sample	I_{sc} (mA)	I_{max}(mA)	V_{oc}(V)	V_{max}(V)
$ZnAl_2O_3$	46.223	42.334	0.145	0.136
$ZnCdO_4$	45.541	42.241	0.178	0.167
$ZnCoO_2$	42.947	39.414	0.200	0.179
$Zn\ Li_2\ O_2$	45.439	42.038	0.261	0.244
$ZnMgO_2$	44.648	41.534	0.171	0.157

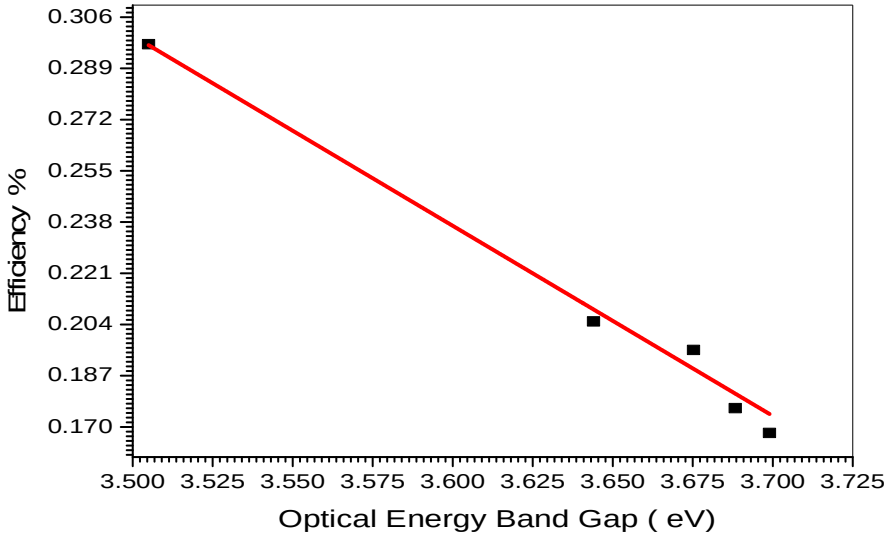

Fig (4.54)the relationship between energy band gap and efficiency of ZnO samples

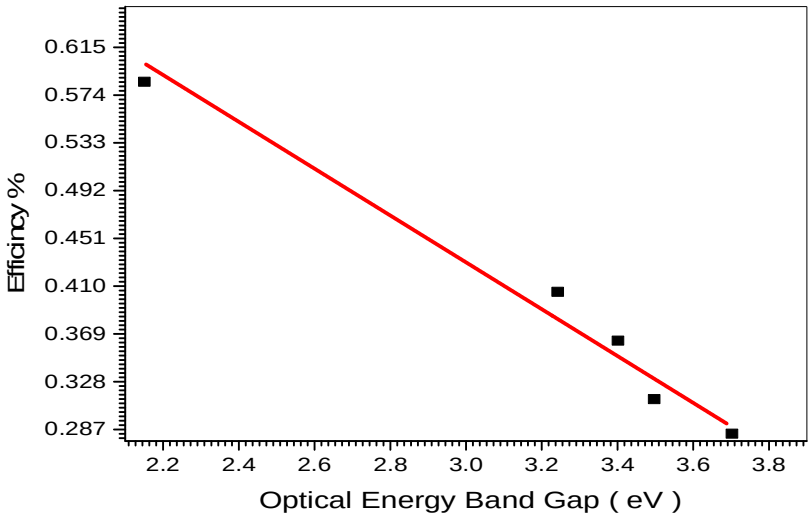

Fig (4.55)the relationship between energy band gap and efficiency of TiO samples

In view of fig (4.59) it is clear that the efficiency decreases upon increasing the energy gap . This agrees with the fact that when the energy gap decreases more photons generated free electrons which increases current which in turn increase the efficiency . It is also important to note that the absorption coefficient increases when decreasing the energy gap in general this signaldecreasing energy gap allows move photons to be absorbed to generated free electrons which increases absorption coefficient ,for Al_2O_3 absorption decreases . This may be because it transparent as for as it consists of extra Oxygen's thus transmit more light which decrees absorption.

Chapter Five

Conclusion and Suggested Future Work

5.1 Conclusion:

The doping process shows that the efficiency increases when the energy gap decreases . The absorption Coefficient increases when the energy gap decreases.

5.2 Suggested Future Work:

- We recommend further work in this area to enhance the dye structure and produce and adjust concentration to produce good performance by finding a common solvent to the dye and the fullerene so that the solvent can be easily evaporated and yield efficient cells .
- The thickness of the cell must be decreased then become thinness for more efficiency.
- The temperature effect on the cells properties could be further investigated as well.
- Other dopant materials can be used to increase the dye photoconductivity

Reference

[1] Dong, S.; Pu, S.; Huang, J. Magnetic field sensing based on magneto-volume variation of magnetic fluids investigated by air-gap Fabry-Pérot fiber interferometers. Appl. Phys. Lett. 2013, 103,doi:10.1063/1.4821104.

[2] Miao, Y.; Wu, J.; Lin, W.; Zhang, K.; Yuan, Y.; Song, B.; Zhang, H.; Liu, B.; Yao, J. Magnetic field tunability of optical microfiber taper integrated with ferrofluid. Opt. Express 2013, 21,29914–29920.

[3] Deng, M.; Liu, D.; Li, D. Magnetic field sensor based on asymmetric optical fiber taper and magnetic fluid. Sens. Actuators A Phys. 2014, 211, 55–59.

[4] Ji, H.; Pu, S.; Wang, X.; Yu, G. Magnetic field sensing based on V-shaped groove filled with magnetic fluids. Appl. Opt. 2012, 51, 1010–1020.

[5] Wang, H.; Pu, S.; Wang, N.; Dong, S.; Huang, J. Magnetic field sensing based on

singlemode-multimode-singlemode fiber structures using magnetic fluids as cladding. Opt. Lett. 2013, 38, 3765–3768.

[6] Wu, J.; Miao, Y.; Lin, W.; Song, B.; Zhang, K.; Zhang, H.; Liu, B.; Yao, J. Magnetic-field sensor based on core-offset tapered optical fiber and magnetic fluid. J. Opt. 2014, 16, doi:10.1088/ 2040-8978/16/7/075705.

[8] Candiani, A.; Argyros, A.; Leon-Saval, S.G.; Lwin, R.; Selleri, S.; Pissadakis, S. A loss-based, magnetic field sensor implemented in a ferrofluid infiltrated microstructure polymer optical fiber. Appl. Phys. Lett. 2014, 104, doi:10.1063/1.4869129 .

[8] Zheng, J.; Dong, X.; Zu, P.; Ji, J.; Su, H.; Shum, P. Intensity-modulated magnetic field sensor based on magnetic fluid and optical fiber gratings. Appl. Phys. Lett. 2013, 103, doi:10.1063/1.4828562.

[9] Yang, D.; Du, L.; Xu, Z.; Jiang, Y.; Xu, J.; Wang, M.; Bai, Y.; Wang, H. Magnetic field sensing based on tilted fiber bragg grating coated with nanoparticle magnetic fluid. Appl. Phys. Lett. 2014, 104, doi:10.1063/1.4864649.

[10] Pu, S.; Dong, S.; Huang, J. Tunable slow light based on magnetic-fluid infiltrated photonic crystal waveguides. J. Opt. 2014, 16, doi:10.1088/2040-8978/16/4/045102.

[11] Kemkar, S.D.; Mahajan, H.S.; Vaidya, M. Ferro fluid based optical fiber switch. In Proceedings of the 56th Dae Solid State Physics Symposium 2011, Tamilnadu, India, 19–23 December 2011; doi:10.1063/1.4710108.

[12] Chieh, J.J.; Yang, S.Y.; Horng, H.E.; Hong, C.-C.; Yang, H.C. Magnetic-fluid optical-fiber modulators via magnetic modulation. Appl. Phys. Lett. 2007, 90, doi:10.1063/1.2716365.

[13] Zu, P.; Chan, C.C.; Koh, G.W.; Lew, W.S.; Jin, Y.; Liew, H.F.; Wong, W.C.; Dong, X. Enhancement of the sensitivity of magneto-optical fiber sensor by magnifying the birefringence of magnetic fluid film with Loyt-Sagnac interferometer. Sens. Actuators B Chem. 2014, 191, 19–23.

[14] Miao, Y.; Liu, B.; Zhang, K.; Zhang, H.; Wang, R.; Liu, Y.; Yao, J. Magneto-optical tunability of magnetic fluid infiltrated microstructured optical fiber. Opt. Laser Technol. 2013, 48, 280–284.

[15] Homa, D.; Pickrell, G. Magnetic sensing with ferrofluid and fiber optic connectors. Sensors 2014, 14, 3891–3896.

[16] Nguyen, L.V.; Hwang, D.; Moon, S.; Moon, D.S.; Chung, Y. High temperature fiber sensor with high sensitivity based on core diameter mismatch. Opt. Express 2008, 16, 11369–11375.

[17] Sun, A.; Wu, Z.; Wan, C.; Yang, C. All-fiber optic acoustic sensor based on multimode-single mode-multimode structure. Optik 2012, 123, 1138–1139.

[18] J. P. Gordon: Phys.Rev. A 8, 14 (1973) 275

[19] I. Brevik: Phys. Rep. 52, 133 (1979) 275

[20] R. Peierls: More Surprises in Theoretical Physics, (Princeton University Press,
Princeton 1991) 275

[21] J. D. Jackson: Classical Electrodynamics (Wiley, New York 1975) 275, 279

[22] L. D. Landau, E. M. Lifshitz, L. P. Pitaevskii: Electrodynamics of Continuous
Media (Pergamon, Oxford 1984) 276, 277, 278

[23] PingSheng: Introduction in Wave Scattering, Localization and Mesoscopic
Physics (Academic, San Diego 1995) 276, 282, 284, 285

[24] Research Group POAN (Ed): New Aspects of Electromagnetic and Acoustic
Wave Diffusion (Springer, Berlin, Heidelberg, 1998) 276

[25] A. Lagendijk, B. A. van Tiggelen: Phys. Rep. 270, 143 (1996) 276

[26] N. B. Baranova, B. Ya. Zel’dovich: JETP Lett. 509, 681 (1994) 278

[27] R. Schlesser, A. Weis: Opt. Lett. 14, 1015 (1992) 278

[28] G. W. ’t Hooft, M. B. van der Mark: Nature 381, 27 (1996) 278

[29] D. F. Nelson: Phys. Rev. Lett. 76, 4713 (1996) 278

[30] Y. Jiang, M. Liu: Phys. Rev. Lett. 77, 1043 (1996) 278

[31] M. F. Bishop, A. A. Maradudin: Phys. Rev. B 14, 3384 (1976) 278

[32] A. Puri, J. L. Birman: Phys. Rev. A 27, 1044 (1983) 278

[33] M. Born, E. Wolf: Principles of Optics (Pergamon, Oxford 1980) 279

[34] R. P. Feynman, R. B. Leighton, M. Sands: The Feynman Lectures on Physics,
Vol. II, Sect. 27–4 (Addison-Wesley, Reading1979) 279
[35] J. A. Stratton: Electromagnetic Theory (McGraw-Hill, New York 1941)
Sect. 2–19 279
[36] G. L. J. A. Rikken, B. A. van Tiggelen: Phys. Rev. Lett. 78, 847 (1997) 279,
280
[37] G. W.'tHooft, G. Nienhuis, J. C. J. Paaschens: Phys. Rev. Lett. 80, 1114
(1998) 280
[38] G. L. J. A. Rikken, B. A. van Tiggelen: Phys. Rev. Lett. 80, 1115 (1998) 280,
290
22. G. L. J. A. Rikken, B. A. van Tiggelen: Nature 381, 54 (1996) 285, 292, 294
[39] I. Campos, J. L. Jim´enez: Eur. J. Phys. 13, 117 (1992) 281
[40] G. W. Ford, S. A. Werner: Phys. Rev. B 18, 6752 (1978) 281
[41] H. C. van de Hulst: Light Scattering by Small Particles (Dover, New York 1981)
281, 285, 299
[42] D. Lacoste, B. A. van Tiggelen, G. L. J. A. Rikken, A. Sparenberg: J. Opt. Soc.
Am. A 15, 1636 (1998) 281, 282, 283, 295
[43] F. Erbacher, R. Lenke, G. Maret: Europhys. Lett. 21, 551 (1993) 284
[44] R. Lenke: Diffusion Multiple de la Lumi`ere: D´estruction de la R´etrodiffusion

Coh´erente par la Rotation Faraday Magn´eto-optique. Ph.D. Thesis, Universit´e
Joseph Fourier, Grenoble (1994) 284
[45] A. S. Martinez, R. Maynard: Phys. Rev. B 50, 3714 (1994) 284, 290
[46] F. C. MacKintosh, S. John: Phys. Rev B 37, 1884 (1988) 284
[47] D. Lacoste, B. A. van Tiggelen: Phys. Rev. E 61, 4556 (2000) 284
[48] J. J. M. Beenakker, G. Scoles, H. F. P. Knaap, R. M. Jonkman: Phys. Lett. 2,
5 (1962) 284
[49] D. Lacoste, B. A. van Tiggelen: Europhys. Lett. 45, 721 (1999) 285, 286, 289,
295
[50] D. Lacoste: Diffusion de la Lumi`eredans les MilieuxMagn´eto-optiquesouChiraux.
Ph.D. Thesis, Universit´e Joseph Fourier, Grenoble (1999) 285, 289
[51] B. A. van Tiggelen: Phys. Rev. Lett. 75, 422 (1995) 285, 289
[52] N. W. Ashcroft, N. D. Mermin: Solid State Physics (Holt, New York 1976)
App. E 285
[53] B. A. van Tiggelen, R. Maynard and Th.M. Nieuwenhuizen: Phys. Rev. E 53,
2881 (1996) 285, 299
[54] J. H. Li, A. A. Lisyansky, T. D. Cheung, D. Livdan, A. Z. Genack: Europhys.
Lett. 22, 675 (1993) 287
[55] G. D¨uchs, A. Sparenberg, G. L. J. A. Rikken, B. A. van Tiggelen: Phys. Rev.
E. 62, 2840 (2000) 290, 291, 292, 293

[56] Berkovski, B. Magnetic Fluids and Applications Handbook; Begell House, Inc.
New York, U.S.A., 1996.
[57] Piso, M. I. J. Magn. Magn. Mater. 1999, 201, 380.
[58] Yamaguchi, H.; Kobori, I.; Kobayashi, N. J.Magn. Magn. Mater. 1999, 201, 260.
[59] Rosensweig, R. E. Nature 1966, 210, 613.
[60] Horng, H. E.; Hong, C. Y.; Yang, S. Y.; Yang, H.C. J. Phys. Chem. Solids 2001, 62, 1749.
[61] Hong, C. Y.; Chen, C. A; Chen, C. H.; Horng,H. E.; Yang, S. Y.; Yang, H. C. Appl. Phys.Letter. 2001, 79, 2360.
[62] Tsebers, A. O. Magn. Gidro. 1982, 18, 42 (inRussian). English translation:
Magnetohydrodynamics, 1983, 18, 345.
[63] Sano, K.; Doi, M. J. Phys. Soc. Jpn. 1983, 52,2810.
[64] Yusuf, N. A. J. Phys. D: Appl. Phys. 1989, 22,1916.
[65] Hong, C. Y. R.; Horng, H. E.; Yang, H. C.;Yeung, W. B. U. S. Pat. No. 5948321.
[66] Horng, H. E.; Hong, C. Y.; Yang, H. C.; Jang, I. J.;Yang, S. Y.; Wu, J. M.; Lee, S. L.; Kuo, F. C., J.Magn. Magn. Mater. 1999, 201, 215.
[67] Hong, C.Y., J. Appl. Phys. 1999, 85, 5962.
[68] Horng, H. E. in preparation.
[69] Jones, G. A.; Niedoba, H. J. Magn. Magn.Mater. 1988, 73, 33.
[70] Jones, G. A.; Moman, A. IEEE Trans. Magn.1990, 26, 1849.
[71] Cernak J.; Macko, P. J. Magn. Magn. Mater.1993, 123, 107.
[72] Wang, Hao, Zhu, Yun, Boyd, C.; Luo, Weili,Cebers, A.; Rosensweig, R. E. Phys. Rev. Lett.1994, 72, 1929.
[73] Ytreberg, F.; Marty, M.; Susan R. Phys. Rev. E2000, 61, 4107.

[74] Hong, C. Y.; Horng, H. E.; Jang, I. J.; Hsu, C.J.; Yao, Y. D.; Yang, H. C. J. Appl. Phys. 1997,81, 4275.

[75] Yang, S. Y.; Jang, I. J.; Horng, H. E.; Hong, C. Y.;Yang, H. C. Magn. Gidro. 2000, 36, 19.

[76] A. J. Epstein, Y. Yang (Eds.), Polymeric and Organic Electronic Materials: fromScientific Curiosity to Applications, MRS Bull. 1997, 22, 13.

[77] Ma, Z., Wang, E., Jarvid, M. E., Henriksson, P., Inganäs, O., Zhang, F. &Andersson, M. R. Synthesis and characterization of benzodithiophene–isoindigo polymers for solar cells. J. Mater. Chem. 22,2306–2314 (2012).

[78]Ali VeyselTunc a Q2 , Antonietta De Sio a, Daniel Riedel b, Felix Deschler b, Enrico Da Como b, Jürgen Parisi a, Elizabeth von Hauff / Molecular doping of low-bandgap-polymer:fullerene solar cells: Effects on transport and solar cells / ORGELE 1435 No. of Pages 7, Model 3G 6 December 2011.

[79]K. Gurunathan et al. / Materials Chemistry and Physics 61 (1999) 173±191.

[80]Xiong Gong1,3, Cesare Soci1, Cuiying Yang1, Alan J Heeger1 and Steven Xiao2 / Enhanced electron injection in polymer light-emitting diodes: polyhedral oligomericsilsesquioxanes as dilute additives / INSTITUTE OF PHYSICS PUBLISHING- JOURNAL OF PHYSICS D: APPLIED PHYSICS - J. Phys. D: Appl. Phys. 39 (2006) 2048–2052 doi:10.1088/0022-3727/39/10/011.

[81]M. Drees, K. Premaratne, W. Graupner,a) and J. R. Heflinb / Creation of a gradient polymer-fullerene interface in photovoltaic devices by thermally controlled interdiffusion - APPLIED PHYSICS LETTERS VOLUME 81, NUMBER 24 9 DECEMBER 2002.

[82] Abdelsakhi .S.M - Using Gum Arabic in Making Solar Cells by Thin Films Instead Of Polymers - IOSR Journal of Applied Physics (IOSR-JAP) ISSN: 2278-4861.Volume 8, Issue 1 Ver. III (Jan. - Feb. 2016), PP 27-32 .

[83] Dong-JooKwak*, Byung-Ho Moon*, Don-Kyu Lee**, Cha-Soo Park*** and Youl-Moon Sung† - Journal of Electrical Engineering & Technology Vol. 6, No. 5, pp. 684~687, 2011 http://dx.doi.org/10.5370/JEET.2011.6.5.684 .

[84] 1Sakina Ibrahim Ali , 2Mubarak DirarAbdallah, 3Sawsan Ahmed Elhouri Ahmed - International Journal of Current Trends in Engineering & Research (IJCTER) e-ISSN 2455–1392 Volume 2 Issue 7, July 2016 pp. 82 – 89 Scientific Journal Impact Factor : 3.468 http://www.ijcter.com .

[85] James A. Marusek - Solar Storm Threat Analysis - Impact, 2007 James A. Marusek .

[86] B.C. Yadav and Ritesh Kumar - Structure, properties and applications of fullerenes / International Journal of Nanotechnology and Applications ISSN 0973-631X Volume 2, Number 1 (2008), pp. 15–24 © Research India Publications http://www.ripublication.com/ijna.htm.

[87] WiHyoung Lee 1,* and Yeong Don Park 2,*- Organic Semiconductor/Insulator Polymer Blends for High-Performance Organic Transistors/Polymers 2014, 6, 1057-1073;doi:10.3390/polym6041057-ISSN-2073-60www.mdpi.com/journal/polymers.

[88] SHI Quan-Min/ Role of TiO2 Nanotube on Improvement of Performance of Hybrid Photovoltaic Devices - CHIN. PHYS. LETT. Vol. 26, No. 1 (2009) 017202.

[89] J.H. Parka-Non-linear I_V characteristics of MEH-PPV patterned on sub-micrometer electrodes/Thin Solid Films 393 (2001. 129_131).

[90] A. Mayer, S. Scully, B. Hardin, M. Rowell, M. McGehee, (2007).Polymer-based solar cells, Materials Today 10.

[91] Ma, Z., Wang, E., Jarvid, M. E., Henriksson, P., Inganäs, O., Zhang, F. &Andersson, M. R. Synthesis and characterization of benzodithiophene–isoindigo polymers for solar cells. J. Mater. Chem. 22,2306–2314 (2012).

[92] Kang B, Tan L W and Silva S R P 2008 Appl. Phys. Lett.93 133302

[93] Yoo I, Lee M, Lee C, Kim D W, Moon I S and Hwang D H 2005 Synth. Met. 153 97

[94] Tao C, Ruan S P, Xie G H, Kong X Z, Shen L, Meng F X, Liu C X, Zhang X D, Dong W and Chen W Y 2009 Appl. Phys. Lett. 94 043311.

[95] A. Bewick, M. Fleischmann, H.R. Thirsk, Trans. Faraday Soc., 58 (1962) 2200.

[96] S. Bijani, R. Schrebler, E.A. Dalchiele, M. Gabás, L. Martínez, and J. R. Ramos-Barrado, J. Phys. Chem. C, 115 (2011) 21373.

[97] T.L. Barr, Y.L. Liu, J. Phys. Chem. Solids, 50 (1989) 657.

[98] B.D. Cullity, Elements of X-ray Diffraction 2nd Ed. (Addi-son-Wesley, Reading, MA, 1978).

[99] W. Vallejo, J. Clavijo, Brazilian Journal of Physics, 40 (2010) 30.

[100] P. O'Brien, D. J. Otway, and J. R.Walsh, Thin Solid Films, 315 (1998) 57.

[101] R. Henríquez, P. Grez, E. Muñoz, H. Gómez, J.A. Badán, R.E. Marotti, E.A. Dalchiele, Thin Solid Films, 518 (2010) 1774.

[102] R. Yoosuf, M.K. Jayaraj, Sol Energy Mater Sol Cells, 89 (2005) 85.

[103] R.E. Marotti, C.D. Bojorge, E. Broitman, H.R. Cánepa, J.A. Badán, E.A. Dalchiele, A.J. Gellman, Thin Solid Films, 517 (2008) 1077.

[104] A. Akkari, C. Guasch, M. Castange, J. Mater. Sci., 46 (2011) 6285.